HoloGRAV 2012
Swansea 18 April 2012

Holographic Bottom-up models for QCD.

Elias Kiritsis

University of Crete APC, Paris

Bibliography

Based on earlier work by

Umut Gursoy, Liuba Mazzanti, George Michalogiorgakis, Fransesco Nitti, arXiv:1006.5461 [hep-th]

recent work with:

Matti Jarvinnen (Crete) arXiv:1112.1261 [hep-ph]

and ongoing work with:

T. Alho (Helsinki), D. Arean (SISSA) I. Iatrakis (Crete), M. Jarvinnen (Crete), K. Kajantie (Helsinki), K. Tuominnen (Helsinki).

Introduction

• There are two main reasons for developing bottom up holographic models:

♠ It is a way of exploring the holographic landscape, by matching gravitational actions with IR strong coupling behavior (equilibrium properties, phase diagrams and dynamics (like transport))

♠ It is the main tool for developing the concept of Effective Holographic Theories (EHT): the holographic analogue of EFT.

• In the case of YM and QCD , the scope is to go beyond the top-down models and model the relevant physics all the more realistically.

This review will deal with:

• A bottom up model for YM

• A tachyon-condensation inspired model for flavor

• A model for QCD in the Veneziano limit.

The holographic models: glue

For YM, ihQCD is a well-tested holographic, string-inspired bottom-up model with action

Gursoy+Kiritsis+Nitti, 2007, Gubser+Nelore, 2008

$$\mathcal{S}_{\rm g} = M^3 N_c^2 \int d^5x \sqrt{g} \left[R - \frac{4}{3}(\partial\phi)^2 + V_g(\phi) \right]$$

- $g_{\mu\nu}$ is dual to $T_{\mu\nu}$

- ϕ is dual to $tr[F^2]$.

We expect that these two operators capture the important part of the dynamics of the YM vacuum. The vacuum saddle point is given by a Poincaré-invariant metric, and radially depended dilaton.

$$ds^2 = e^{2A(r)}(dr^2 + \eta_{\mu\nu}dx^\mu dx^\nu)$$

- The potential $V_g \leftrightarrow$ QCD β-function

- $A \to \log \mu$ energy scale.

• $e^{\phi} \to \lambda$ 't Hooft coupling

In the UV $\lambda \to 0$ and

$$V_g(\lambda) = V_0 + V_1\ \lambda + V_2\ \lambda + \mathcal{O}(\lambda^3)$$

In the IR $\lambda \to \infty$ and

$$V_g \sim \lambda^{\frac{4}{3}} \sqrt{\log \lambda} + \cdots$$

• This was chosen after analysing all possible asymptotics and characterising their behavior.

The IR asymptotics is uniquely fixed by asking for confinement, discrete spectra and asymptotically linear glueball trajectories.

Gursoy+Kiritsis+Nitti

• With an appropriate tuning of two parameters in V_g the model describes well both $T = 0$ properties (spectra) as well as thermodynamics.

YM Entropy

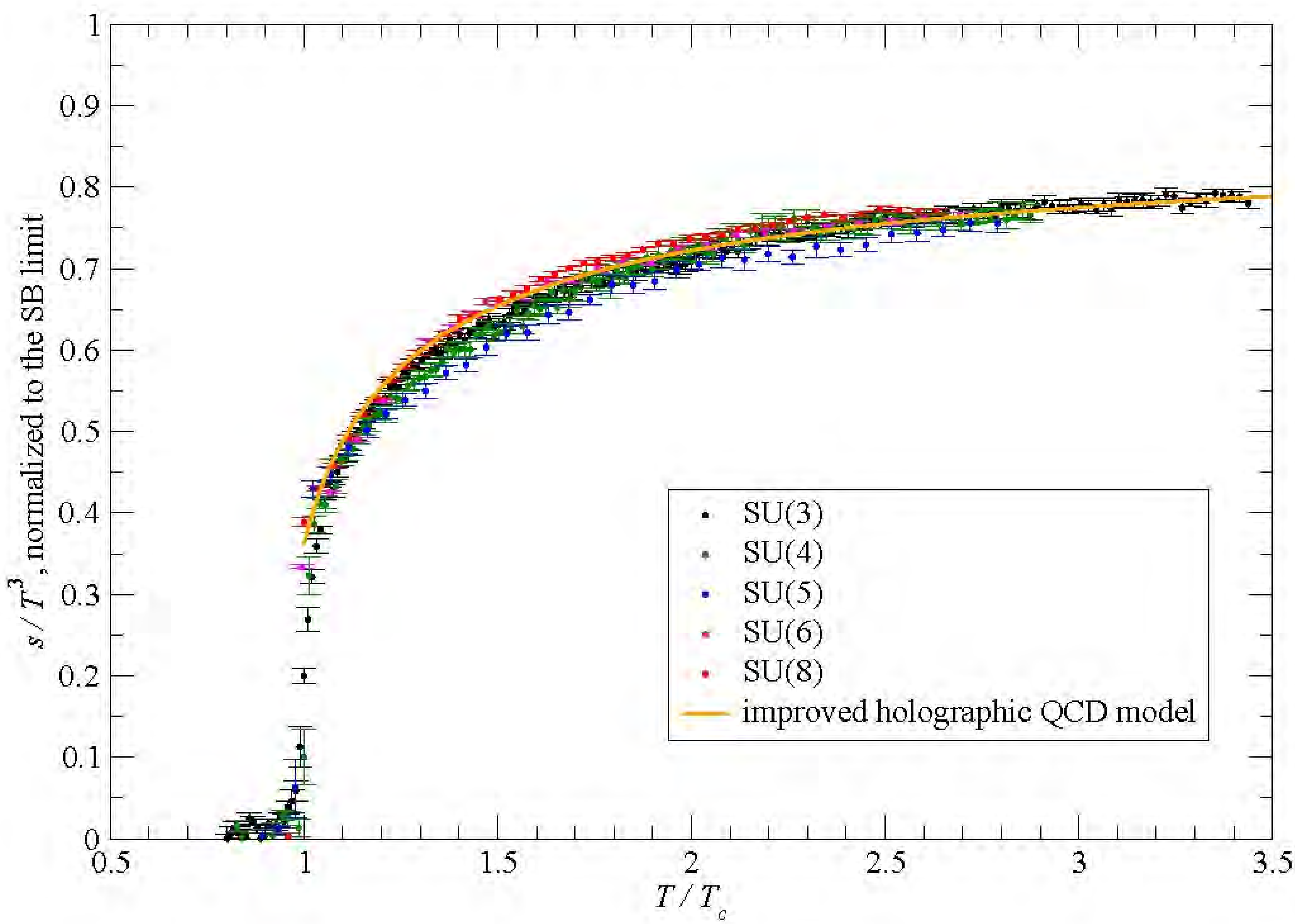

Figure 4: (Color online) Same as in fig. 1, but for the s/T^3 ratio, normalized to the SB limit.

From M. Panero, arXiv:0907.3719

Equation of state

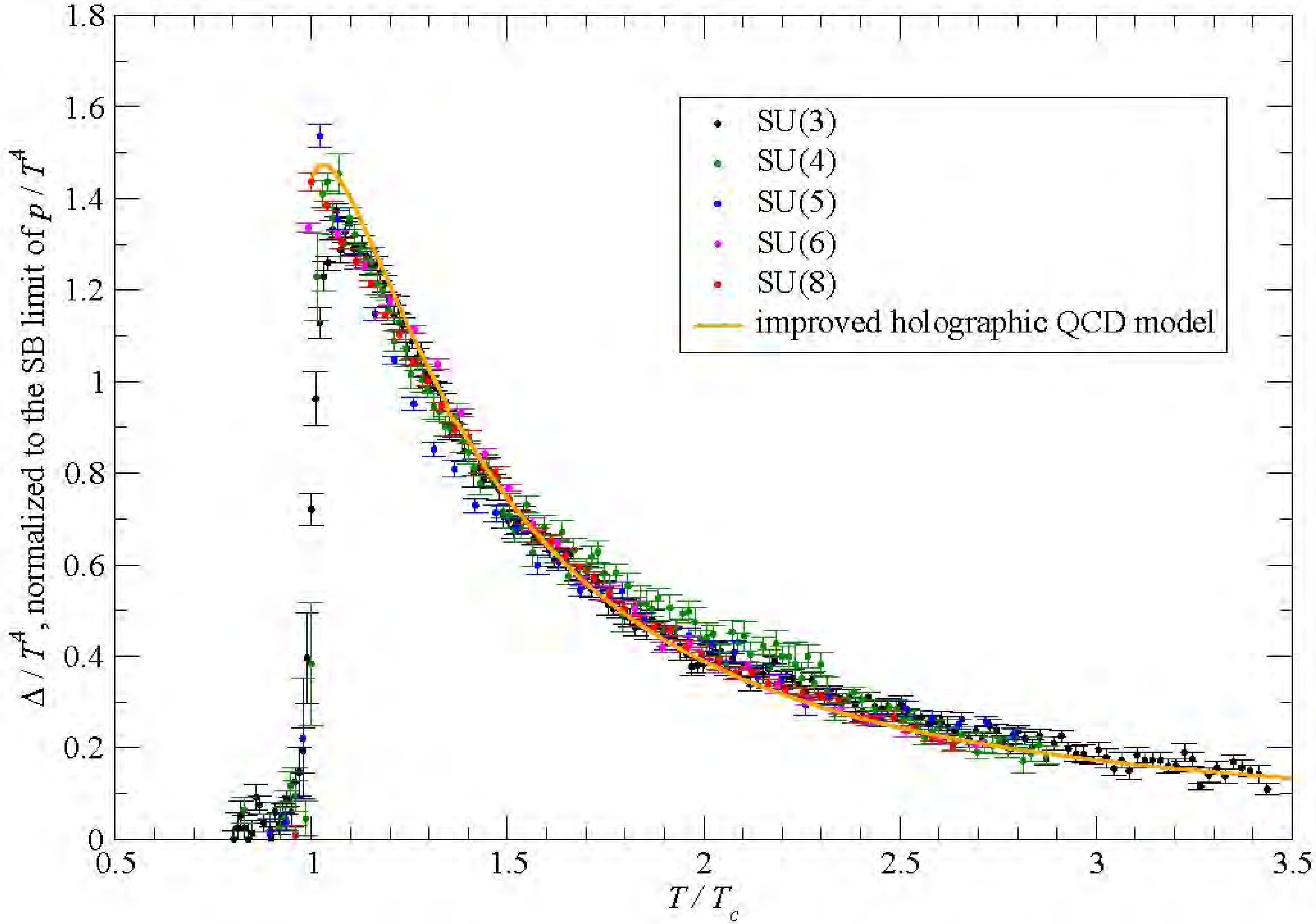

Figure 2: (Color online) Same as in fig. 1, but for the Δ/T^4 ratio, normalized to the SB limit of p/T^4.

From M. Panero, arXiv:0907.3719

The sound speed

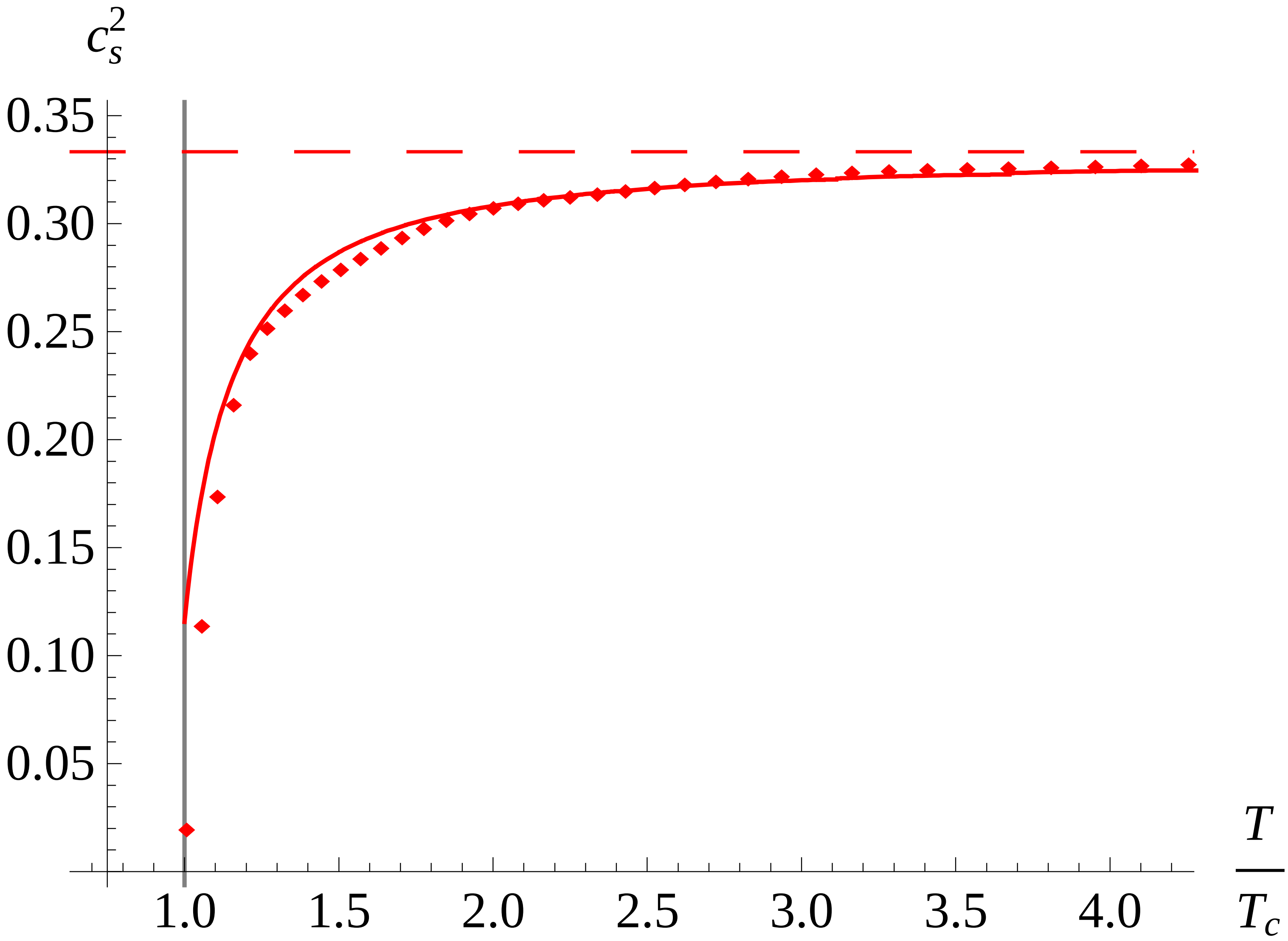

The holographic models: flavor

- Fundamental quarks arise from $D4$-$\bar{D}4$ branes in 5-dimensions.

$$D4 - D4 \quad \text{strings} \quad \rightarrow \quad A_\mu^L \quad \leftrightarrow \quad J_\mu^L = \bar\psi_L \sigma_\mu \psi_L$$

$$\overline{D4} - \overline{D4} \quad \text{strings} \quad \rightarrow \quad A_\mu^R \quad \leftrightarrow \quad J_\mu^R = \bar\psi_R \bar\sigma_\mu \psi_R$$

$$D4 - \overline{D4} \quad \text{strings} \quad \rightarrow \quad T \quad \leftrightarrow \quad \bar\psi_L \psi_R$$

- For the vacuum structure only the tachyon is relevant.

- An action for the tachyon motivated by the Sen action has been advocated as the proper dynamics of the chiral condensate, giving in general all the expected features of χSB.

Casero+Kiritsis+Paredes

$$\mathcal{S}_{\text{TDBI}} = -N_f N_c M^3 \int d^5x \; V_f(T) \; e^{-\phi} \sqrt{-\det(g_{ab} + \partial_a T \partial_b T)}$$

- It has been tested in a 6d asymptotically-AdS confining background (with constant dilaton) due to Kuperstein+Sonneschein.

Iatrakis+Kiritsis+Paredes

It was shown to have the following properties:

- Confining asymptotics of the geometry trigger chiral symmetry breaking.

- A Gell-Mann-Oakes-Renner relation is generically satisfied.

- The Sen DBI tachyon action with $V \sim e^{-T^2}$ asymptotics induces linear Regge trajectories for mesons.

- The Wess-Zumino (WZ) terms of the tachyon action, computed in string theory, produce the appropriate flavor anomalies, include the axial $U(1)$ anomaly and η'-mixing, and implement a holographic version of the Coleman-Witten theorem.

- The dynamics determines the chiral condensate uniquely a s function of the bare quark mass.

- The mass of the ρ-meson grows with increasing quark mass.

- By adjusting the same parameters as in QCD (Λ_{QCD}, m_{ud}) a good fit can be obtained of the light meson masses.

The chiral vacuum structure

- We take the potential to be the flat space one

$$V = V_0 \, e^{-T^2}$$

with a maximum at $T = 0$ and a minimum at $T = \infty$.

- Near the boundary $z = 0$, the solution can be expanded in terms of two integration constants as:

$$\tau = c_1 z + \frac{\pi}{6} c_1^3 z^3 \log z + c_3 z^3 + \mathcal{O}(z^5)$$

- c_1, c_3 are related to the quark mass and condensate.

- At the tip of the cigar, the generic behavior of solutions is

$$\tau \sim constant_1 + constant_2 \sqrt{z - z_\Lambda}$$

- With special tuned condition there is a one-parameter family of diverging solutions in the IR depending on a single parameter:

$$\tau = \frac{C}{(z_\Lambda - z)^{\frac{3}{20}}} - \frac{13}{6\pi C}(z_\Lambda - z)^{\frac{3}{20}} + \dots$$

• This is the correct "regularity condition" in the IR as τ is allowed to diverge only at the tip.

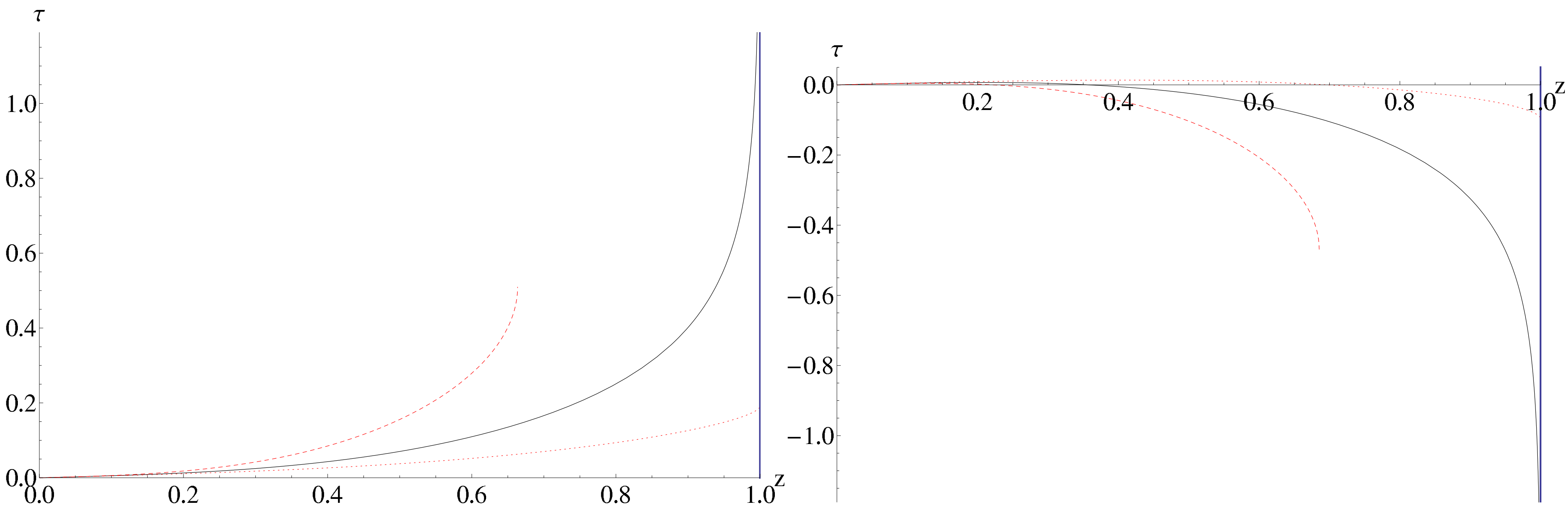

All the graphs are plotted using $z_\Lambda = 1$, $\mu^2 = \pi$ and $c_1 = 0.05$. The tip of the cigar is at $z = z_\Lambda = 1$. On the left, the solid black line represents a solution with $c_3 \approx 0.3579$ for which τ diverges at z_Λ. The red dashed line has a too large c_3 ($c_3 = 1$) - such that there is a singularity at $z = z_s$ where $\partial_z \tau$ diverges while τ stays finite. This is unacceptable since the solution stops at $z = z_s$ where the energy density of the flavor branes diverges. The red dotted line corresponds to $c_3 = 0.1$; this kind of solution is discarded because the tachyon stays finite everywhere. The plot in the right is done with the same conventions but with negative values of $c_3 = -0.1, -0.3893, -1$. For $c_3 \approx -0.3893$ there is a solution of the differential equation such that τ diverges to $-\infty$. This solution is unstable.

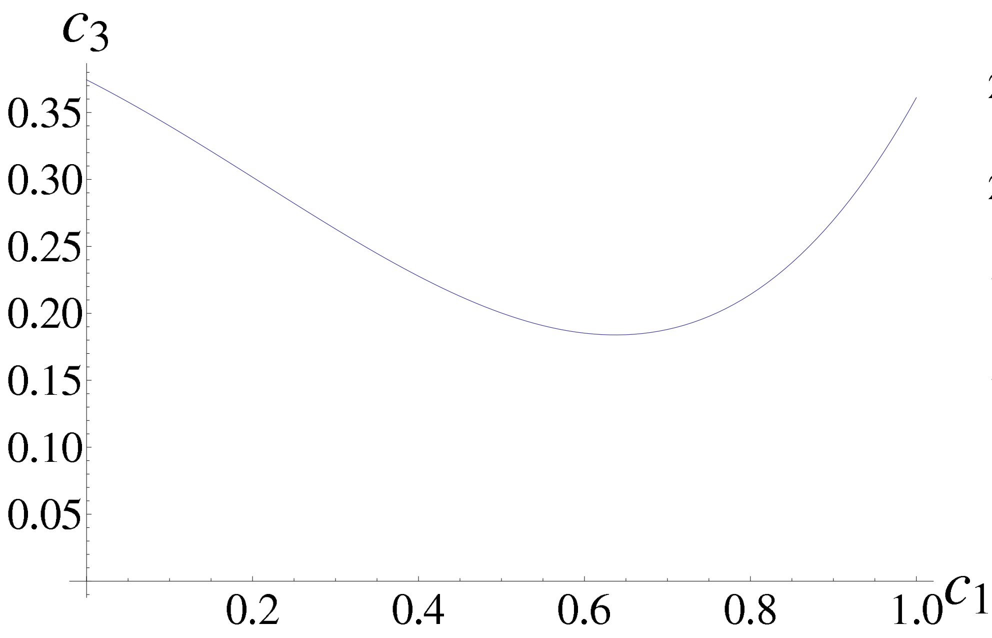

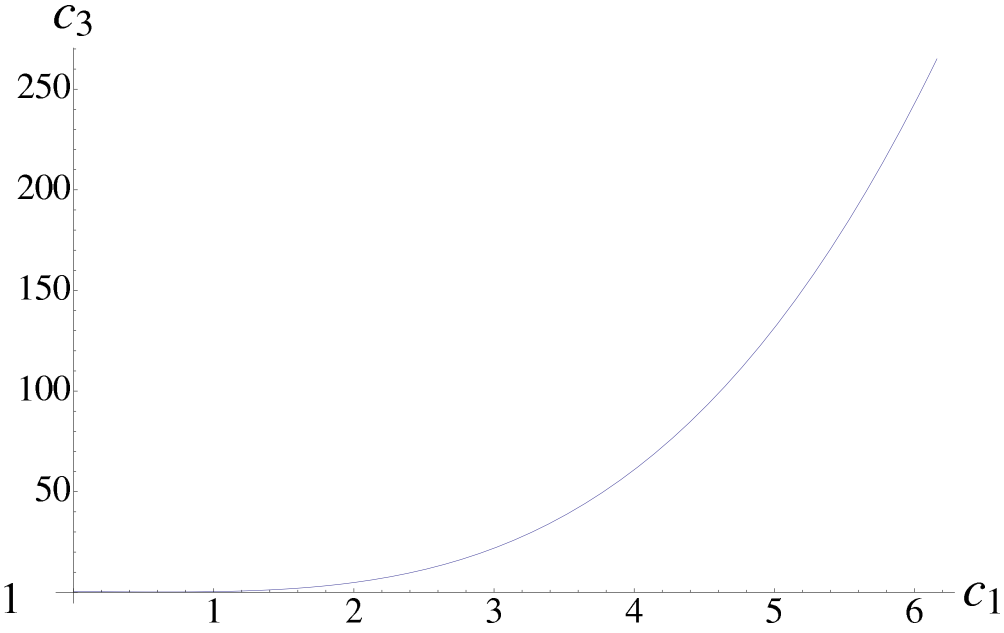

- Chiral symmetry breaking is manifest.

Chiral restauration at deconfinement

- In the deconfined phase, the bulk metric is that of a bh.

- The branes now are allowed to enter the horizon without recombining.

- To avoid intermediate singularities of the solution the boundary conditions must be tuned so that tachyon is finite at the horizon.

- Near the horizon the correct solution behaves as a one-parameter family

$$\tau = c_T - \frac{3c_T}{5z_T}(z_T - z) - \frac{9c_T}{200z_T}(8 + \mu^2 {c_T}^2)(z_T - z)^2 + \dots$$

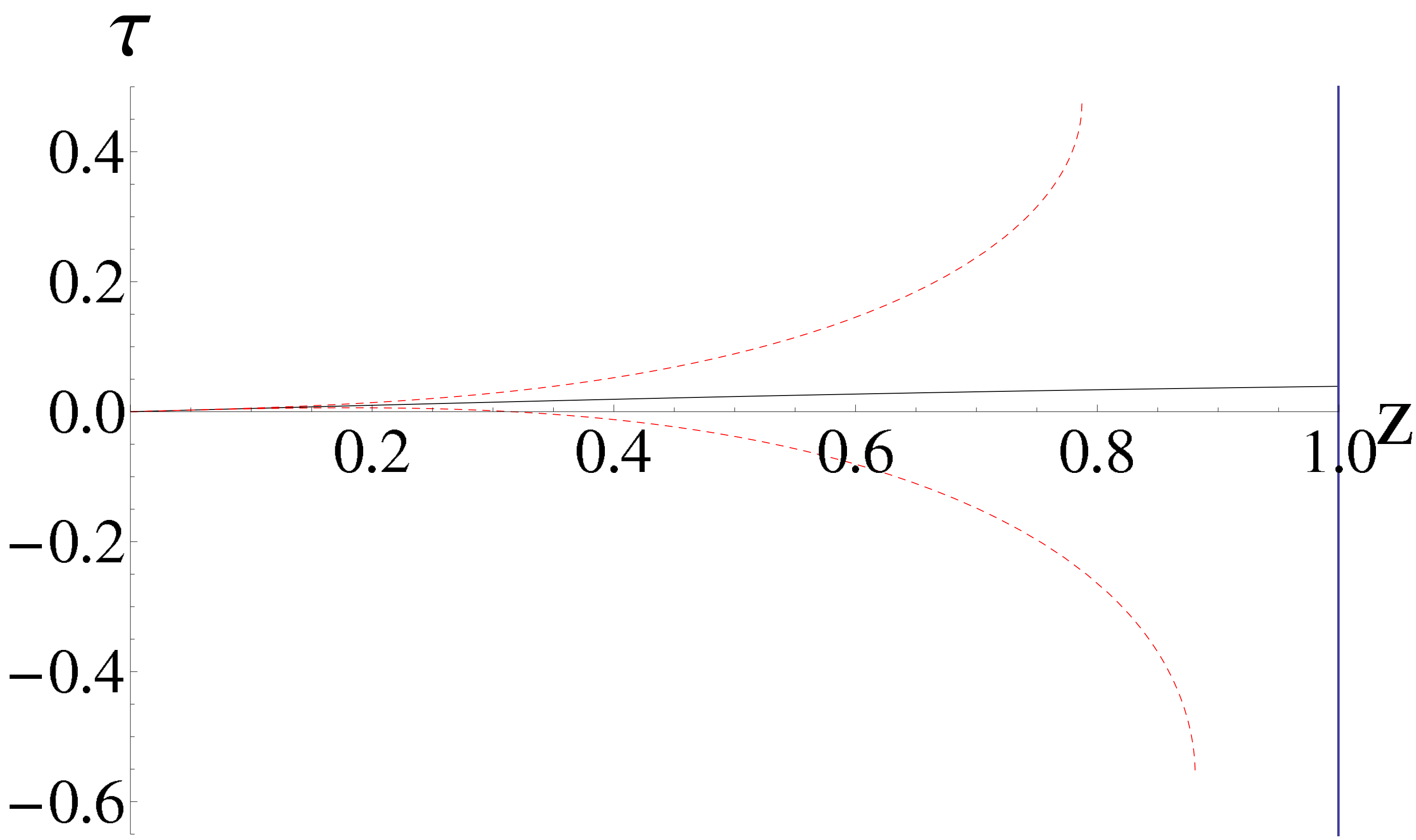

Plots corresponding to the deconfined phase. We have taken $c_1 = 0.05$. The solid line displays the physical solution $c_3 = -0.0143$ whereas the dashed lines ($c_3 = -0.5$ and $c_3 = 0.5$) are unphysical and end with a behavior of the type $\tau = k_1 - k_2\sqrt{z_s - z}$.

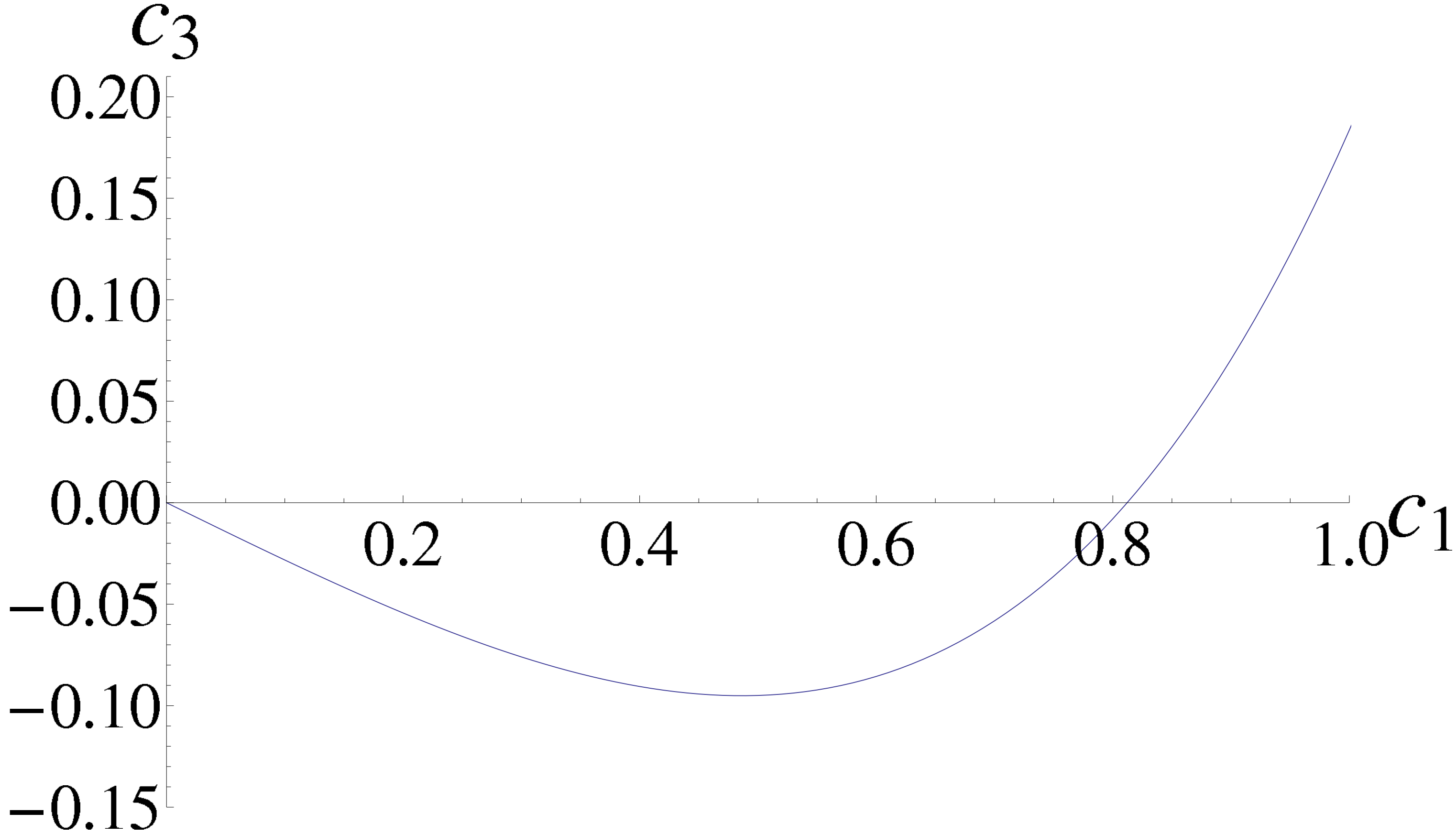

These plots give the values of c_3 determined numerically by demanding the correct IR behavior of the solution, as a function of c_1.

Jump of the condensate at the phase transition

- From holographic renormalization we obtain

$$\langle \bar{q}q \rangle = \frac{1}{\beta}(2\pi\alpha' \mathcal{K} R^3 \lambda)\left(-4c_3 + \left(\frac{m_q}{\beta}\right)^3 \mu^2 (1+\alpha)\right) \quad , \quad m_q = \beta\ c_1$$

- We calculate the jump at the phase transition that is scheme independent for a fixed quark mass.

$$\Delta\langle \bar{q}q \rangle \equiv \langle \bar{q}q \rangle_{conf} - \langle \bar{q}q \rangle_{deconf} = -4\frac{1}{\beta}(2\pi\alpha' \mathcal{K} R^3 \lambda)\Delta c_3$$

- This is equivalent to Δc_3

• We plot it as a function of the quark mass.

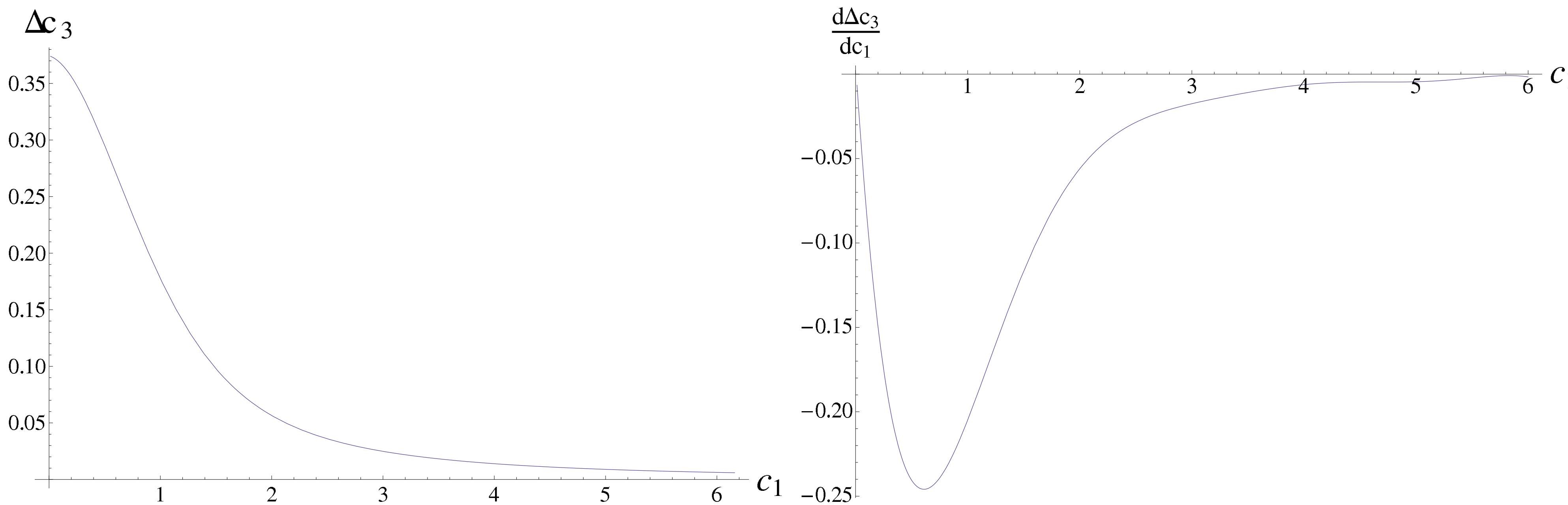

The finite jump of the quark condensate and its derivative with respect to c_1 when the confinement-deconfinement transition takes place. The important features appear when $m_q \sim \Lambda_{QCD}$

Meson spectra

For the vectors

$$z_\Lambda m_V^{(1)} = 1.45 + 0.718c_1 , \qquad z_\Lambda m_V^{(2)} = 2.64 + 0.594c_1 , \qquad z_\Lambda m_V^{(3)} = 3.45 + 0.581c_1 ,$$
$$z_\Lambda m_V^{(4)} = 4.13 + 0.578c_1 , \qquad z_\Lambda m_V^{(5)} = 4.72 + 0.577c_1 , \qquad z_\Lambda m_V^{(6)} = 5.25 + 0.576c_1 .$$

For the axial vectors:

$$z_\Lambda m_A^{(1)} \approx 2.05 + 1.46c_1 , \qquad z_\Lambda m_A^{(2)} \approx 3.47 + 1.24c_1 , \qquad z_\Lambda m_A^{(3)} \approx 4.54 + 1.17c_1 ,$$
$$z_\Lambda m_A^{(4)} \approx 5.44 + 1.13c_1 , \qquad z_\Lambda m_A^{(5)} \approx 6.23 + 1.11c_1 , \qquad z_\Lambda m_A^{(6)} \approx 6.95 + 1.10c_1 .$$

For the pseudoscalars:

$$z_\Lambda m_P^{(1)} \approx \sqrt{3.53c_1^2 + 6.33c_1} , \qquad z_\Lambda m_P^{(2)} \approx 2.91 + 1.40c_1 , \qquad z_\Lambda m_P^{(3)} \approx 4.07 + 1.27c_1 ,$$
$$z_\Lambda m_P^{(4)} \approx 5.04 + 1.21c_1 , \qquad z_\Lambda m_P^{(5)} \approx 5.87 + 1.17c_1 , \qquad z_\Lambda m_P^{(6)} \approx 6.62 + 1.15c_1 .$$

For the scalars:

$$z_\Lambda m_S^{(1)} = 2.47 + 0.683c_1 , \qquad z_\Lambda m_S^{(2)} = 3.73 + 0.488c_1 , \qquad z_\Lambda m_S^{(3)} = 4.41 + 0.507c_1 ,$$
$$z_\Lambda m_S^{(4)} = 4.99 + 0.519c_1 , \qquad z_\Lambda m_S^{(5)} = 5.50 + 0.536c_1 , \qquad z_\Lambda m_S^{(6)} = 5.98 + 0.543c_1 .$$

- Valid up to $c_1 \sim 1$.
- In qualitative agreement with lattice results

Laerman+Schmidt., Del Debbio+Lucini+Patela+Pica, Bali+Bursa

Mass dependence of f_π

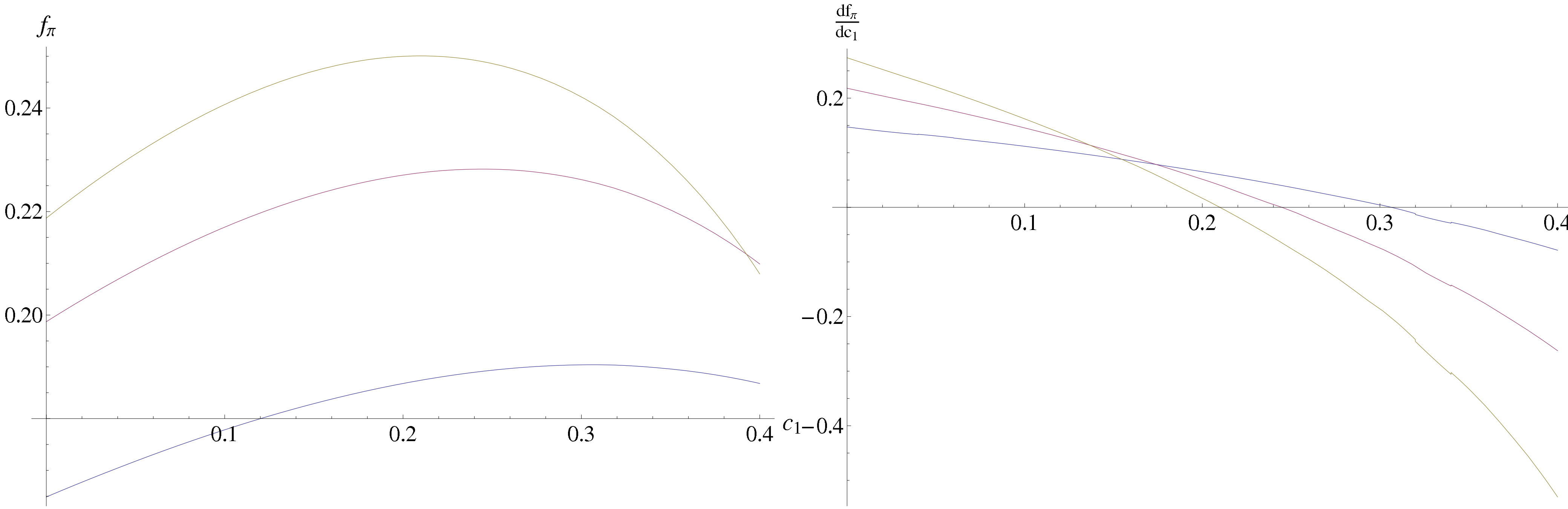

The pion decay constant and its derivative as a function of c_1 - the quark mass. The different lines correspond to different values of k. From bottom to top (on the right plot, from bottom to top in the vertical axis) $k = \frac{12}{\pi^2}, \frac{24}{\pi^2}, \frac{36}{\pi^2}$. The pion decay constant comes in units of z_Λ^{-1}.

Linear Regge Trajectories

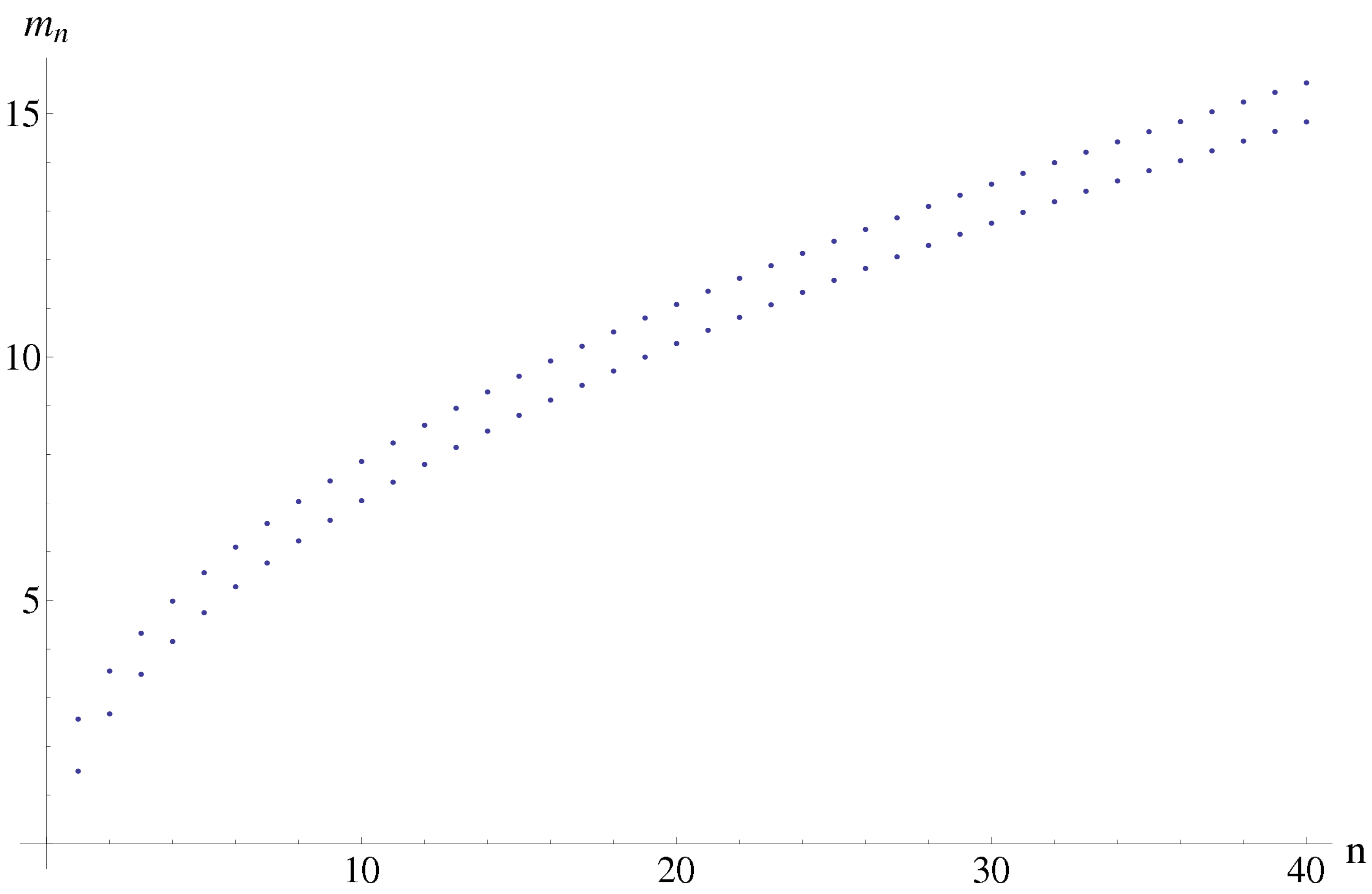

Results corresponding to the forty lightest vector states with $c_1 = 0.05$ and $c_1 = 1.5$.

The Veneziano limit

• The 't Hooft limit

$$N_c \to \infty, \qquad l = g^2_{\text{YM}} N_c \to \text{fixed}$$

always samples the quenched approximation as N_f is kept fixed as $N_c \to \infty$.

• The proper limit in order to study phenomena where flavor is important in the large N_c approximation is the limit introduced by Veneziano

$$N_c \to \infty \quad , \quad N_f \to \infty \quad , \quad \frac{N_f}{N_c} = x \to \text{fixed} \quad , \quad \lambda = g^2_{\text{YM}} N_c \to \text{fixed}$$

• In terms of the dual string theory, the boundaries of diagrams are not suppressed anymore: surfaces with an arbitrary number of boundaries contribute at the same order (for the flavor singlet sector).

The Banks-Zaks region

- The QCD β function in the V-limit is

$$\dot{\lambda} = \beta(\lambda) = -b_0\lambda^2 + b_1\lambda^3 + \mathcal{O}(\lambda^4) \quad , \quad b_0 = \frac{2}{3}\frac{(11-2x)}{(4\pi)^2} \quad , \quad \frac{b_1}{b_0^2} = -\frac{3}{2}\frac{(34-13x)}{(11-2x)^2}$$

- The Banks-Zaks region is $x = 11/2 - \epsilon$ with $\epsilon \ll 1$ and positive. We obtain a fixed point of the β-function at $\lambda_* \simeq \frac{(8\pi)^2}{75}\epsilon + \mathcal{O}(\epsilon^2)$ which is trustable in perturbation theory, as λ_* can be made arbitrarily small.
- The mass operator, $\bar{\psi}_L\psi_R$ has now dimension smaller than three, from the perturbative anomalous dimension (in the V-limit)

$$-\frac{d\log m}{d\log\mu} \equiv \gamma = \frac{3}{(4\pi)^2}\lambda + \frac{(203-10x)}{12\,(4\pi)^4}\lambda^2 + \mathcal{O}(\lambda^3, N_c^{-2})$$

- Extrapolating to lower x we expect the phase diagram

Fusion

The idea is to put together the two ingredients in order to study the chiral dynamics and its backreaction to glue.

$$\mathcal{S} = M^3 N_c^2 \int d^5x \sqrt{g} \left[R - \frac{4}{3}\frac{(\partial\lambda)^2}{\lambda^2} + V_g(\lambda) \right] -$$

$$-N_f N_c M^3 \int d^5x V_f(\lambda, T) \sqrt{-\det(g_{ab} + h(\lambda)\partial_a T \partial_b T)}$$

with $V_f(\lambda, T) = V_0(\lambda) \exp(-a(\lambda)T^2)$

- V-limit: $N_c \to \infty$ with $x = N_f/N_c$ fixed: backreacted system.

- Probe limit $x \to 0 \Rightarrow V_g$ fixed as before.

- We must choose $V_0(\lambda), a(\lambda), h(\lambda)$.

♠ The simplest and most reasonable choices, compatible with glue dynamics do the job!

The effective potential

For solutions $T = T_* = constant$ the relevant non-linear action simplifies

$$\mathcal{S} = M^3 N_c^2 \int d^5x \sqrt{g} \left[R - \frac{4}{3}\frac{(\partial\lambda)^2}{\lambda^2} + V_g(\lambda) - xV_f(\lambda, T) \right]$$

$$V_{\text{eff}}(\lambda) = V_g(\lambda) - xV_f(\lambda, T_*) = V_g(\lambda) - xV_0(\lambda)\exp(-a(\lambda)T_*^2)$$

• Minimizing for T_* we obtain $T_* = 0$ and $T_* = \infty$. The effective potential for λ is

♠ $T_* = 0$, $V_{eff} = V_g(\lambda) - xV_0(\lambda)$

♠ $T_* = \infty$, $V_{eff} = V_g(\lambda)$ with no fixed points.

$$V_{\text{eff}}(\lambda) = V_g(\lambda) - x V_0(\lambda)$$

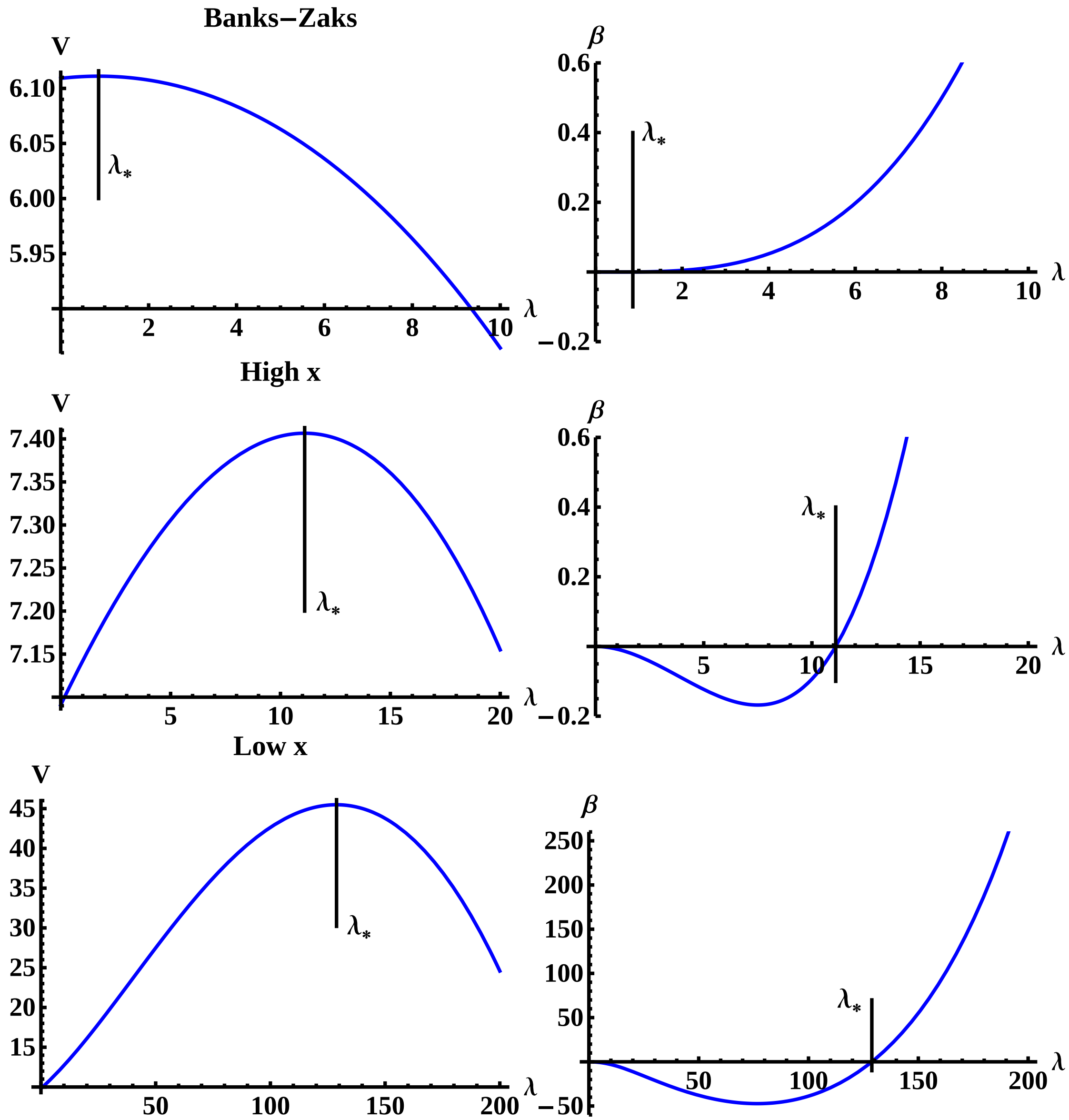

Two possibilities: (a) The maximum exists for all x. (b) The maximum exists for $x > x_*$.

Condensate dimension at the IR fixed point

• By expanding the DBI action we obtain the IR tachyon mass at the IR fixed point $\lambda = \lambda_*$ which gives the chiral condensate dimension:

$$-m_{\mathrm{IR}}^2 \ell_{\mathrm{IR}}^2 = \Delta_{\mathrm{IR}}(4 - \Delta_{\mathrm{IR}}) = \frac{24a(\lambda_*)}{h(\lambda_*)(V_g(\lambda_*) - xV_0(\lambda_*))}$$

• Must reach the Breitenlohner-Freedman (BF) bound (horizontal line) at some x_c.

• x_c marks the *conformal phase transition*

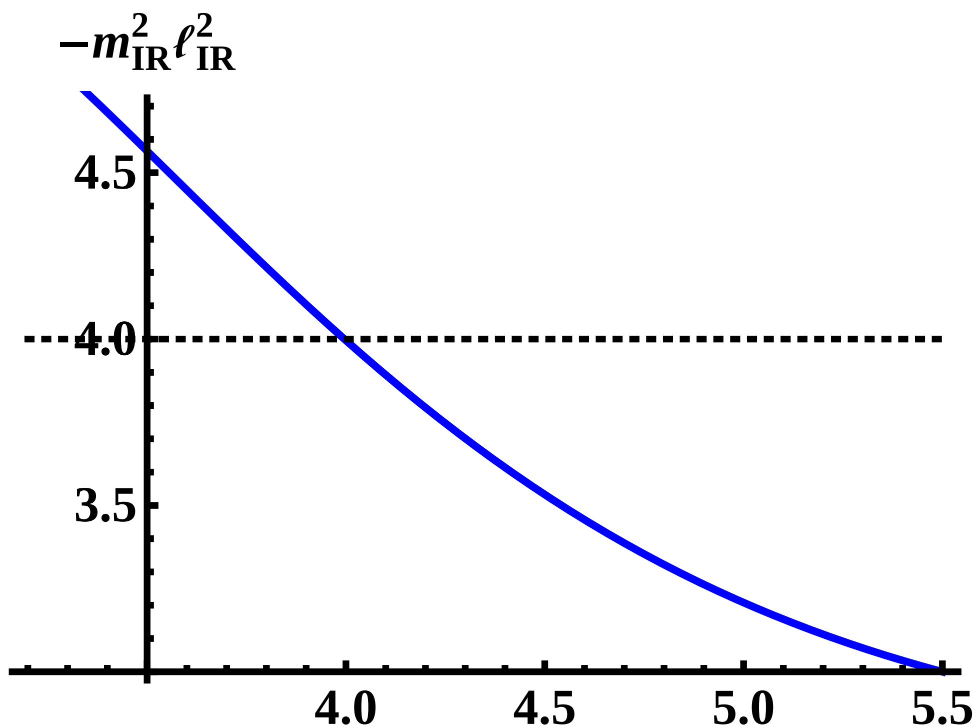

Below the BF bound

• Correlation of the violation of BF bound and the conformal phase transition

• For $\Delta_{\rm IR}(4-\Delta_{\rm IR}) < 4$

$$T(r) \sim m_q r^{4-\Delta_{\rm IR}} + \sigma r^{\Delta_{\rm IR}}$$

• For $\Delta_{\rm IR}(4-\Delta_{\rm IR}) > 4$

$$T(r) \sim C r^2 \sin\left[(\mathrm{Im}\Delta_{\rm IR}) \log r + \phi\right]$$

Two possibilities:

• $x > x_c$: BF bound satisfied at the fixed point $\Rightarrow$ only trivial massless solution ($T \equiv 0$, ChS intact, fixed point hit)

• $x < x_c$: BF bound violated at the fixed point $\Rightarrow$ a nontrivial massless solution exists, which drives the system away from the fixed point.

Conclusion: *phase transition* at $x = x_c$

Matching to QCD: UV

• As $\lambda \to 0$ we can match:

♠ $V_g(\lambda)$ with (two-loop) Yang-Mills β-function.

♠ $V_g(\lambda) - xV_0(\lambda)$ with QCD β-function.

♠ $a(\lambda)/h(\lambda)$ with anomalous dimension of the quark mass/chiral condensate

• The matching allows to mark the BZ point, that we normalize at $x = \frac{11}{2}$.

• After the matching above we are left with a single undetermined parameter in the UV:

$$V_g \sim V_0 + \mathcal{O}(\lambda) \quad , \quad V_0 \sim W_0 + \mathcal{O}(\lambda)$$

$$V_0 - xW_0 = \frac{12}{\ell_{UV}^2}$$

• At finite temperature, W_0 will be fixed from the number of UV degrees of freedom.

Matching to QCD: IR

• In the IR, the tachyon has to diverge $\Rightarrow$ the tachyon action $\propto e^{-T^2}$ becomes small

♠ $V_g(\lambda) \simeq \lambda^{\frac{4}{3}}\sqrt{\lambda}$ chosen as for Yang-Mills, so that a "good" IR singularity exists etc.

♠ $V_0(\lambda)$, $a(\lambda)$, and $h(\lambda)$ chosen to produce tachyon divergence: there are several possibilities.

♠ The phase structure is essentially independent of IR choices.

Choice I:

$$V_g(\lambda) = 12 + \frac{44}{9\pi^2}\lambda + \frac{4619}{3888\pi^4}\frac{\lambda^2}{(1+\lambda/(8\pi^2))^{2/3}}\sqrt{1+\log(1+\lambda/(8\pi^2))}$$

$$V_f(\lambda, T) = V_0(\lambda)e^{-a(\lambda)T^2}$$

$$V_0(\lambda) = \frac{12}{11} + \frac{4(33-2x)}{99\pi^2}\lambda + \frac{23473 - 2726x + 92x^2}{42768\pi^4}\lambda^2$$

$$a(\lambda) = \frac{3}{22}(11-x)$$

$$h(\lambda) = \frac{1}{\left(1+\frac{115-16x}{288\pi^2}\lambda\right)^{4/3}}$$

For which in the IR

$$T(r) \sim T_0 \exp\left[\frac{81\ 3^{5/6}(115-16x)^{4/3}(11-x)}{812944\ 2^{1/6}}\frac{r}{R}\right] \quad , \quad r \to \infty$$

R is the IR scale of the solution. T_0 is the control parameter of the UV mass.

Choice II:

$$a(\lambda) = \frac{3}{22}(11-x)\frac{1+\frac{115-16x}{216\pi^2}\lambda+\frac{\lambda^2}{\lambda_0^2}}{(1+\lambda/\lambda_0)^{4/3}}$$

$$h(\lambda) = \frac{1}{(1+\lambda/\lambda_0)^{4/3}}$$

for which in the IR

$$T(r) \sim \frac{27\ 2^{3/4}3^{1/4}}{\sqrt{4619}}\sqrt{\frac{r-r_1}{R}} \quad , \quad r \to \infty$$

R is the IR scale of the solution. r_1 is the control parameter of the UV mass.

Varying the model

"prediction" for x_c

After fixing UV coefficients from QCD, there is still freedom in choosing the leading coefficient of V_0 at $\lambda \to 0$ and the IR asymptotics of the potentials

Thick blue $\to V_I$

Thin red $\to V_{II}$

Resulting variation of the edge of conformal window

$3.7 \lesssim x_c \lesssim 4.2$

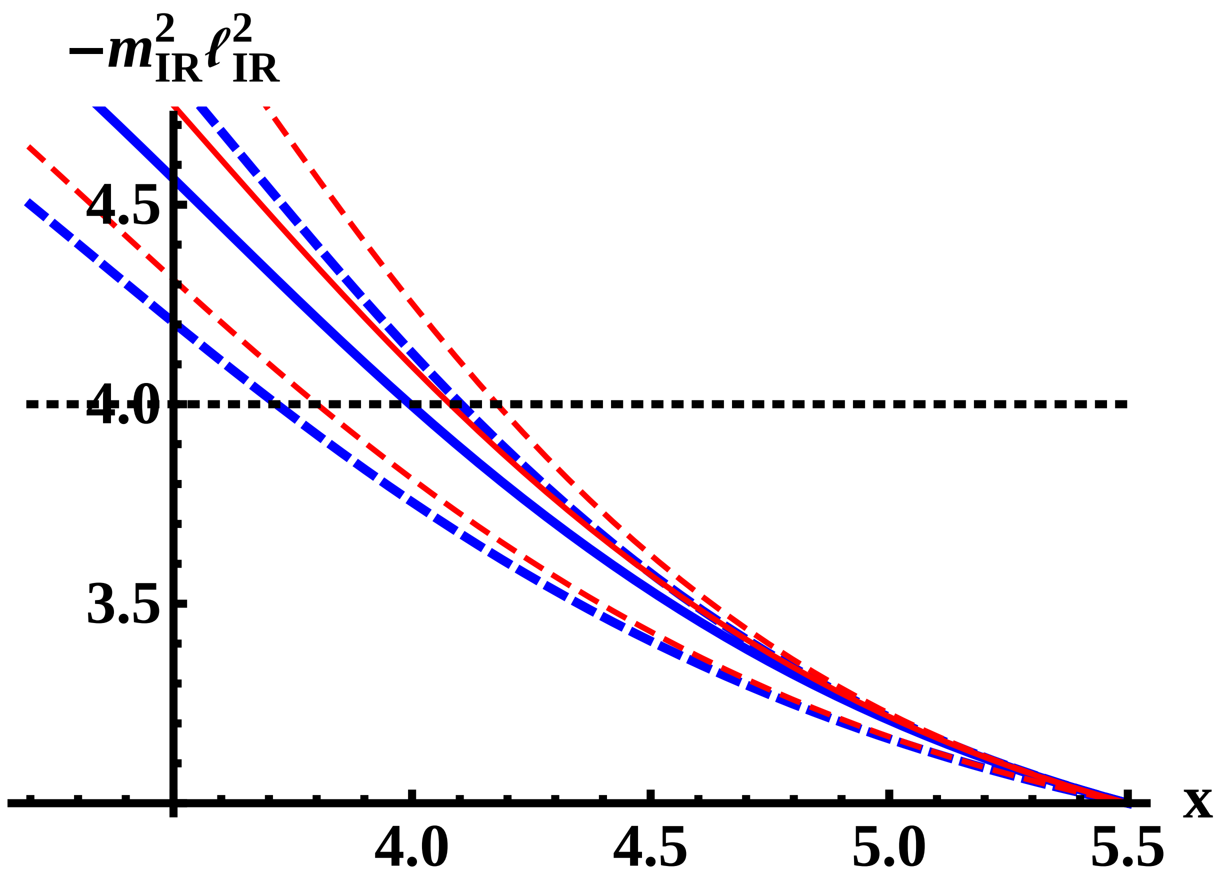

Comparison to previous “guesses”

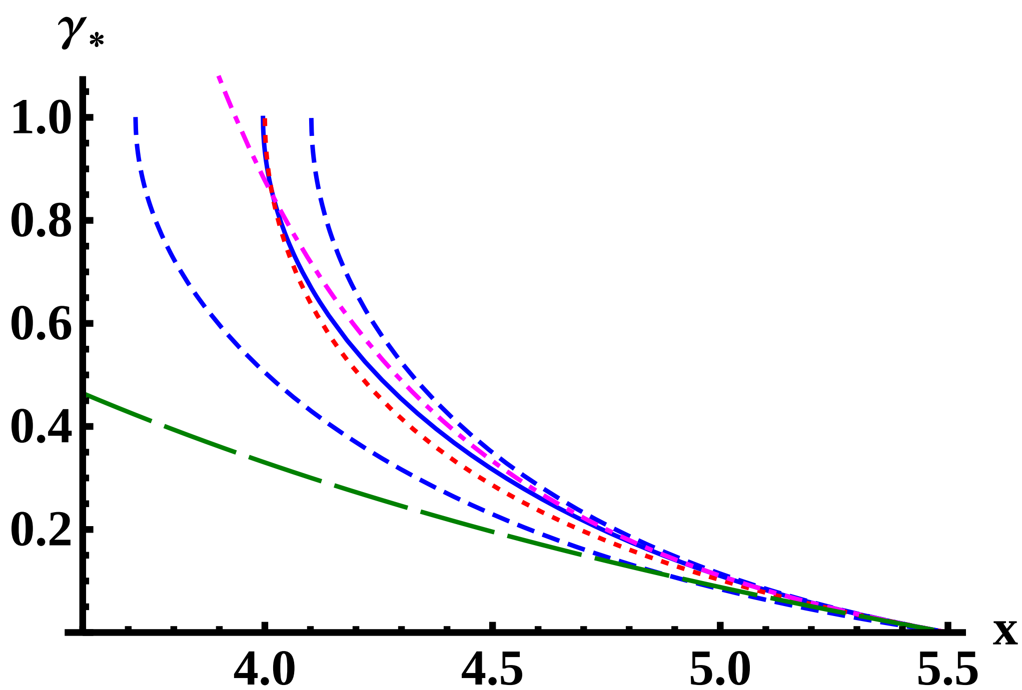

The anomalous dimension of the quark mass at the IR fixed point as a function of x within the conformal window in various approaches.

The solid blue curve is our result for the potential I.

The dashed blue lines show the maximal change as W_0 is varied from 0 (upper curve) to 24/11 (lower curve).

The dotted red curve is the result from a Dyson-Schwinger analysis, the dot-dashed magenta curve is the prediction of two-loop perturbative QCD, and the long-dashed green curve is based on an all-orders β-function.

Holographic β-functions

The second order equations for the system of two scalars plus metric can be written as first order equations for the β-functions

Gursoy+Kiritsis+Nitti

$$\frac{d\lambda}{dA} = \beta(\lambda, T) \quad , \quad \frac{dT}{dA} = \gamma(\lambda, T)$$

The equations of motion boil down to two partial non-linear differential equations for β, γ.

Such equations have also branches as for DBI and non-linear scalar actions the relation of $e^{-A}A'$ with the potentials is a polynomial equation of degree higher than two.

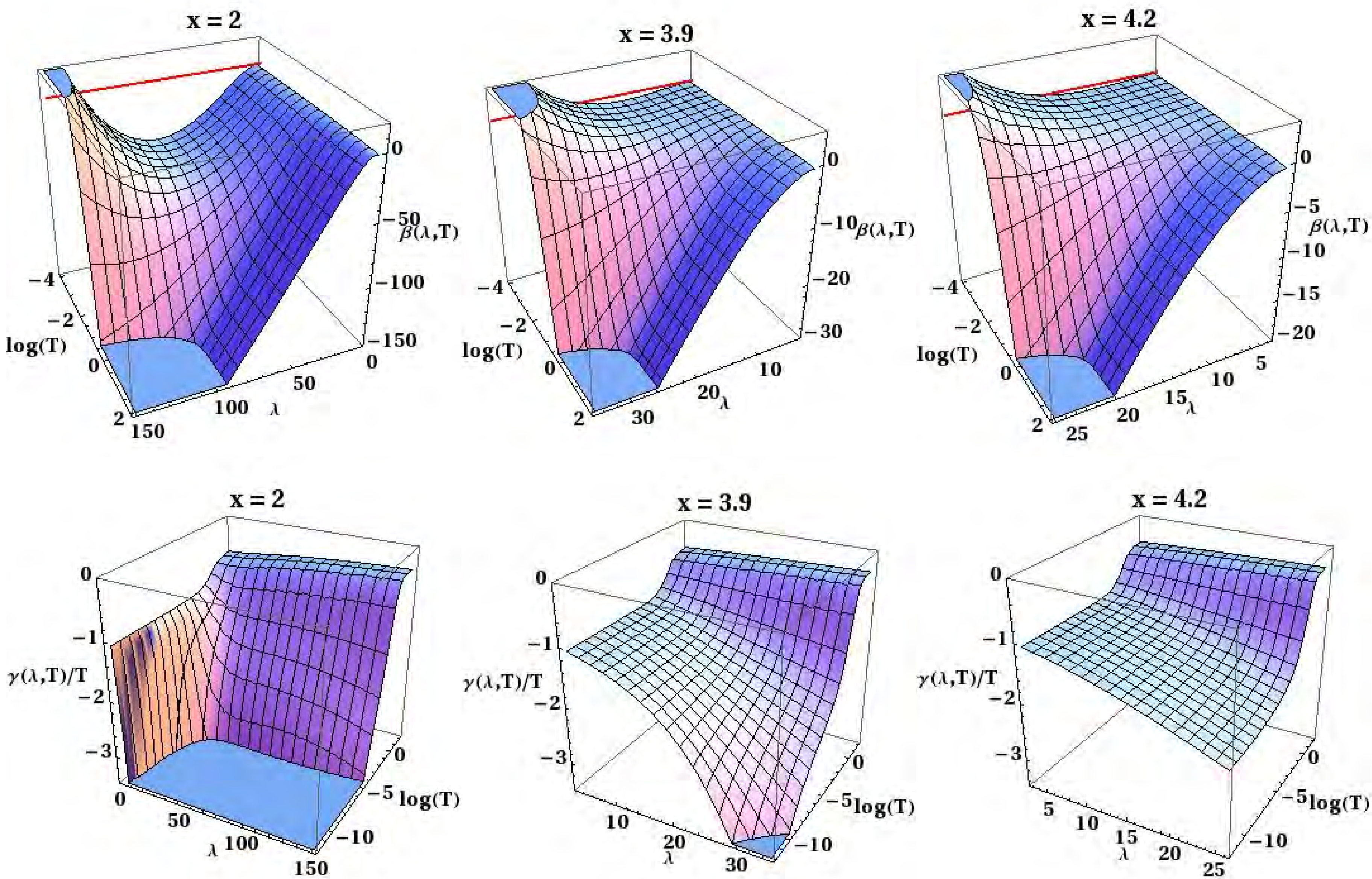

The red lines are added on the top row at $\beta = 0$ in order to show the location of the fixed point.

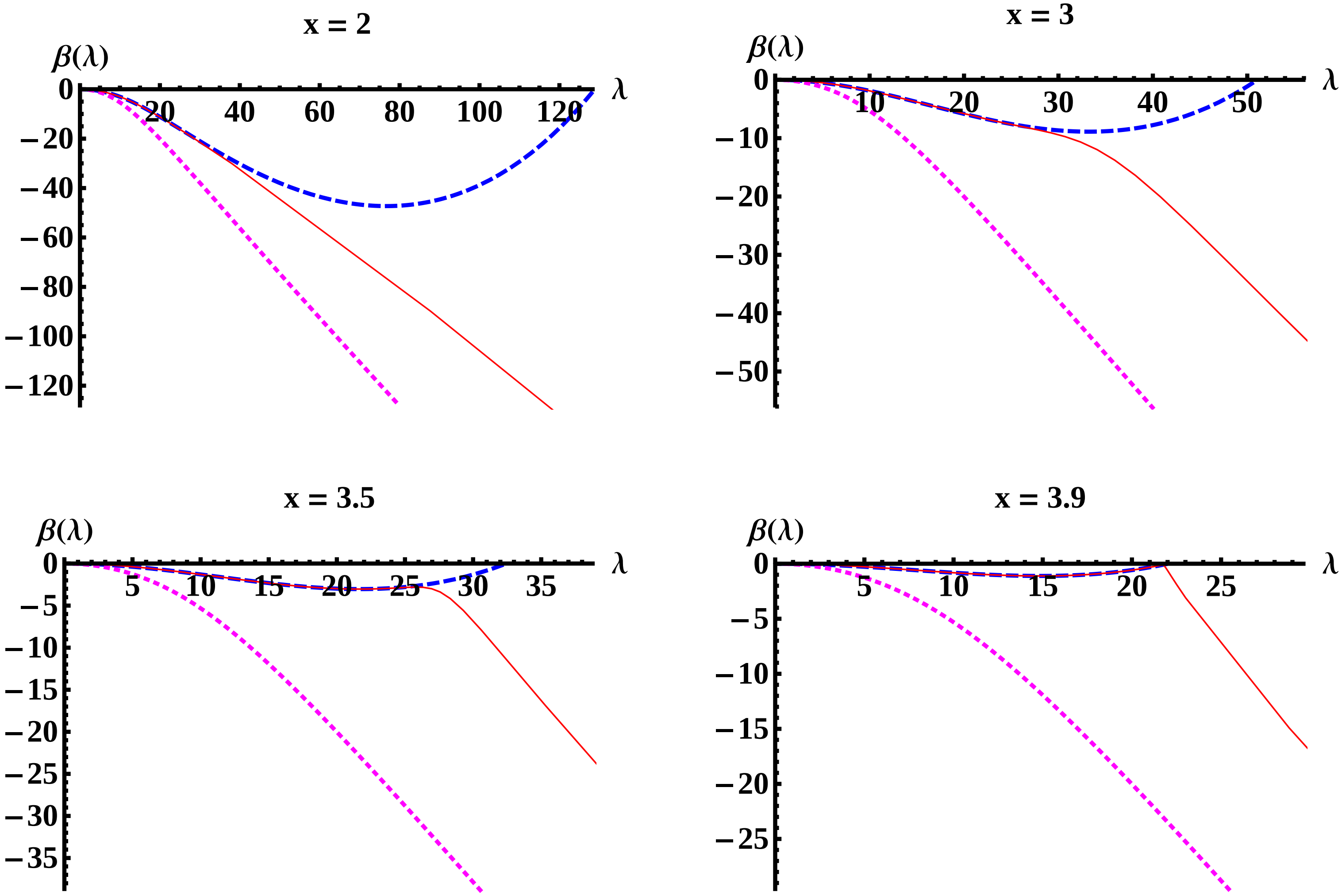

The β-functions for vanishing quark mass for various values of x. The red solid, blue dashed, and magenta dotted curves are the β-functions corresponding to the full numerical solution $(d\lambda/dA)$ along the RG flow, the potential $V_{\rm eff} = V_g - xV_{f0}$, and the potential V_g, respectively.

Parameters

• A theory with a single relevant (or marginally relevant) coupling like YM has no parameters.

• The same applies to QCD with massless quarks.

• QCD with all quarks having mass m has a single (dimensionless) parameter : $\frac{m}{\Lambda_{QCD}}$.

• After various rescalings this single parameter can be mapped to the parameter T_0 that controls the diverging tachyon in the IR.

• There is also x that has become continuous in the large N_c limit.

UV mass vs T_0 and r_1

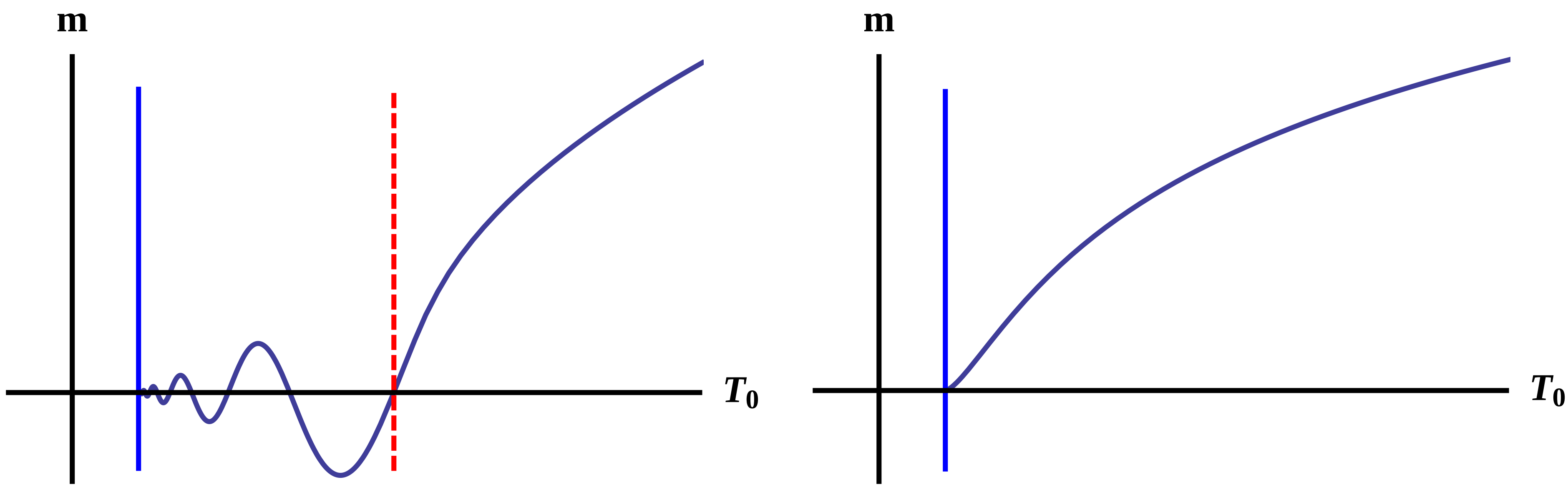

• Left figure: Plot of the UV Mass parameter m, as a function of the IR T_0 scale, for $x < x_c$.

• Right figure: Similar plot for $x \geq x_c$. The vertical solid blue and dashed red lines show where corresponding lines are intersected in previous figures.

• Such plots are sketched from the numerics, analytical expansions and some guesses.

• The tachyon starts at the boundary, evolves into the sinusoidal form for a while, and then at the end diverges. Similar behavior seen at

Kutasov+Lin+Parnachev

• Different solutions differ in the region in which they are sinusoidal, and it is this region that controls their number of zeros.

• For the n-th solution, the tachyon changes sign n times times before diverging in the IR.

• At $m = 0$ there is an ∞ number of saddle point solutions (reflecting the Efimov minima)

• They may appear even in the absence of a IR fixed point

• By adding a double trace interaction $(\bar{\psi}\psi)^2$, and by tuning its coupling, such solutions can become true ground states.

The free energy

The free energy difference between the ChS and ChSB $m_q = 0$ solutions
Chiral symmetry breaking solution favored whenever it exists ($x < x_c$)

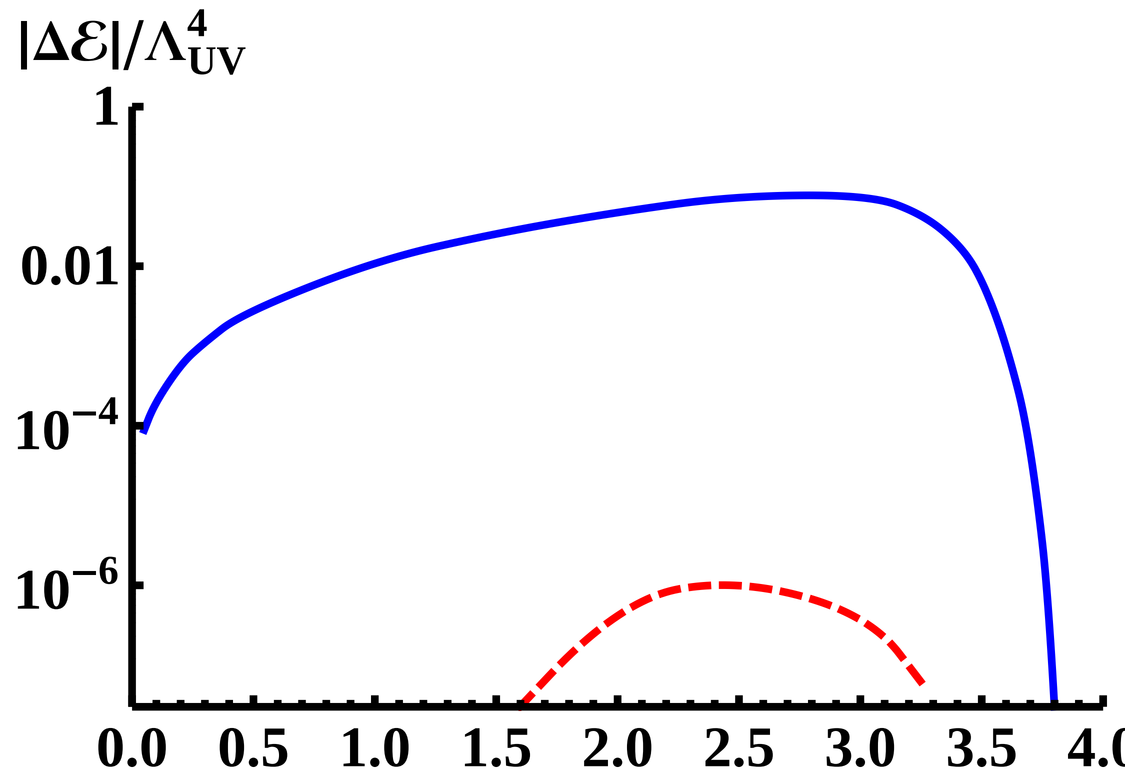

- The Efimov minima have free energies ΔE_n with

$$\Delta E_0 > \Delta E_1 > \Delta E_2 > \cdots$$

Outlook

• Several issues not mentioned here will be explored in the talks by Matti Jarvinen ($T = 0$) and Kimo Tuominen ($T > 0$).

There are many directions that need to be explored:

• The meson spectra at $T = 0$. Singlet mesons will mix with appropriate glueballs. Is the σ-meson a dilaton?.

• Computation of the S parameter for technicolor applications.

• Study energy loss of quarks in QGP (with full backreaction).

• The parameter x resembles somewhat the doping parameter in high-Tc superconductivity. Mesons should be thought of as Cooper pairs of axial charge.

• Study the phase diagram at finite density.

• "Model building": Construction of realistic technicolor models.

.

Thank you

Sen's tachyon DBI action

- The flavor action is the (coinciding) $D_4 - \bar{D}_4$ action:

$$S[T, A^L, A^R] = S_{DBI} + S_{WZ}$$

$$S_{DBI} = \int drd^4x \, \frac{N_c}{l} \, \mathbf{Str} \left[V(T) \left(\sqrt{-\det\left(g_{\mu\nu} + D_{\{\mu}T^\dagger D_{\nu\}}T + F^L_{\mu\nu}\right)} + \right.\right.$$

$$\left.\left. + \sqrt{-\det\left(g_{\mu\nu} + D_{\{\mu}T^\dagger D_{\nu\}}T + F^R_{\mu\nu}\right)} \right) \right]$$

$$D_\mu T \equiv \partial_\mu T - iTA^L_\mu + iA^R_\mu T \quad , \quad D_\mu T^\dagger \equiv \partial_\mu T^\dagger - iA^L_\mu T^\dagger + iT^\dagger A^R_\mu$$

transforming covariantly under flavor gauge transformations

$$T \to V_R \; T \; V_L^\dagger \quad , \quad A^L \to V_L(A^L - iV_L^\dagger dV_L)V_L^\dagger \quad , \quad A^R \to V_R(A^R - iV_R^\dagger dV_R)V_R^\dagger$$

- For the vacuum structure and spectrum $Str = Tr$.

- The tachyon potential in flat space can be computed from boundary CFT.

A simple glue background

Take a simple non-critical confining background:

$$S = \int d^6x \sqrt{g_{(6)}} \left[e^{-2\phi} \left(\mathcal{R} + 4(\partial\phi)^2 + \frac{c}{\alpha'} \right) - \frac{1}{2}\frac{1}{6!} F_{(6)}^2 \right] \; ,$$

Consider the AdS_6 soliton, a solution of non-critical string theory

$$ds_6^2 = \frac{R^2}{z^2} \left[dx_{1,3}^2 + f_\Lambda^{-1} dz^2 + f_\Lambda \, d\eta^2 \right] \quad , \quad f_\Lambda = 1 - \frac{z^5}{z_\Lambda^5} \quad , \quad z \in [0, z_\Lambda]$$

$$F_{(6)} = \frac{Q_c}{\ell_s} \sqrt{-g_{(6)}} \, d^6x \quad , \quad e^\phi = \frac{1}{Q_c} \sqrt{\frac{2c}{3}}$$

Sonnenschein+Kuperstein (04)

- η is periodic

$$\eta \sim \eta + \delta\eta \; , \qquad \delta\eta = \frac{4\pi}{5} z_\Lambda = \frac{2\pi}{M_{KK}} \; . \quad , \quad R^2 = \frac{30}{c} \ell_s^2$$

The deconfined phase

• We consider the theory at non-zero temperature by compactifying to Euclidean time t_E. When both circles t_E and η are compactified, there is a second solution competing with the thermal gas solution :

$$ds_6^2 = \frac{R^2}{z^2}\left[-f_T dt^2 + dx_3^2 + \frac{dz^2}{f_T} + d\eta^2\right] \quad , \quad f_T = 1 - \frac{z^5}{z_T^5}$$

• z_T is related to the temperature as:

$$t_E \sim t_E + \delta t_E \ , \qquad\qquad \delta t_E = \frac{4\pi}{5} z_T = \frac{1}{T} \ .$$

• There is a deconfining first order phase transition at

$$T_c = \frac{M_{KK}}{2\pi} = \frac{5}{4\pi\, z_\Lambda}$$

• For $T < T_c$, the confining solution is preferred and, conversely the black-hole solution dominates for $T > T_c$.

A "warmup" bottom-up model of flavor

• We consider N_f $D_4 + \bar{D}_4$ branes at a fixed η, and we will neglect the coordinate of the branes transverse to the η circle.

• We will take $T = \tau \ \cdot \ 1$

$$V = \mathcal{K}\, e^{-\frac{\mu^2}{2}\tau^2}$$

$$\mathbf{A}_{MN} = g_{MN} + \frac{2\pi\ell_s^2}{g_V^2} F^{(i)}_{MN} + \pi\ell_s^2 \lambda \left((D_M T)^*(D_N T) + (D_N T)^*(D_M T)\right)$$

• Parameters: R, z_Λ, ℓ_s, g_V, λ, $\mathcal{K}$, μ and β.

$$m_q = \beta\ c_1 \quad , \quad \tau(z) \sim c_1\ z + \mathcal{O}(z^3)$$

μ can be eliminated by redefining τ , and we also have

$$\frac{R^2\mu^2}{2\pi\ell_s^2\lambda} = 3 \quad , \quad \frac{(2\pi\ell_s^2)^2\mathcal{K}R}{g_V^4} = \frac{N_c}{12\pi^2} \quad , \quad \frac{(2\pi\ell_s^2)^2\mathcal{K}R^2 l}{\beta^2} = \frac{N_c}{8\pi^2}$$

• We are left with 2+1 parameters that affect the spectra, decay constants and vacuum structure: z_Λ, m_q and $k = \frac{4R^4 g_V^4}{3(2\pi\ell_s^2)^2}$

The chiral vacuum structure

- Set $A_L = A_R = 0$ and derive the scalar $\tau(r)$ equation:

$$\tau'' - \frac{4\pi\, z\, f_\Lambda}{3}\tau'^3 + (-\frac{3}{z} + \frac{f'_\Lambda}{2f_\Lambda})\tau' + \left(\frac{3}{z^2 f_\Lambda} + \pi\, \tau'^2\right)\tau = 0$$

- Near the boundary $z = 0$, the solution can be expanded in terms of two integration constants as:

$$\tau = c_1 z + \frac{\pi}{6} c_1^3 z^3 \log z + c_3 z^3 + \mathcal{O}(z^5)$$

- c_1, c_3 are related to the quark mass and condensate.

- At the tip of the cigar, the generic behavior of solutions is

$$\tau \sim constant_1 + constant_2 \sqrt{z - z_\Lambda}$$

• With special tuned condition there is a one-parameter family of diverging solutions in the IR depending on a single parameter:

$$\tau = \frac{C}{(z_\Lambda - z)^{\frac{3}{20}}} - \frac{13}{6\pi C}(z_\Lambda - z)^{\frac{3}{20}} + \ldots$$

• This is the correct "regularity condition" in the IR as τ is allowed to diverge only at the tip. This is implied by the holographic Coleman-Witten theorem and indicates that the brane-antibrane pair "fuses" at the IR tip.

• To obtain it we must correlate the condensate c_3 to the mass c_1.

• There are always two values of c_3 for a given c_1 that reach the proper solution in the IR, and have opposite signs.

• One of them is always unstable (negative fluctuation masses^2) and is therefore discarded.

.

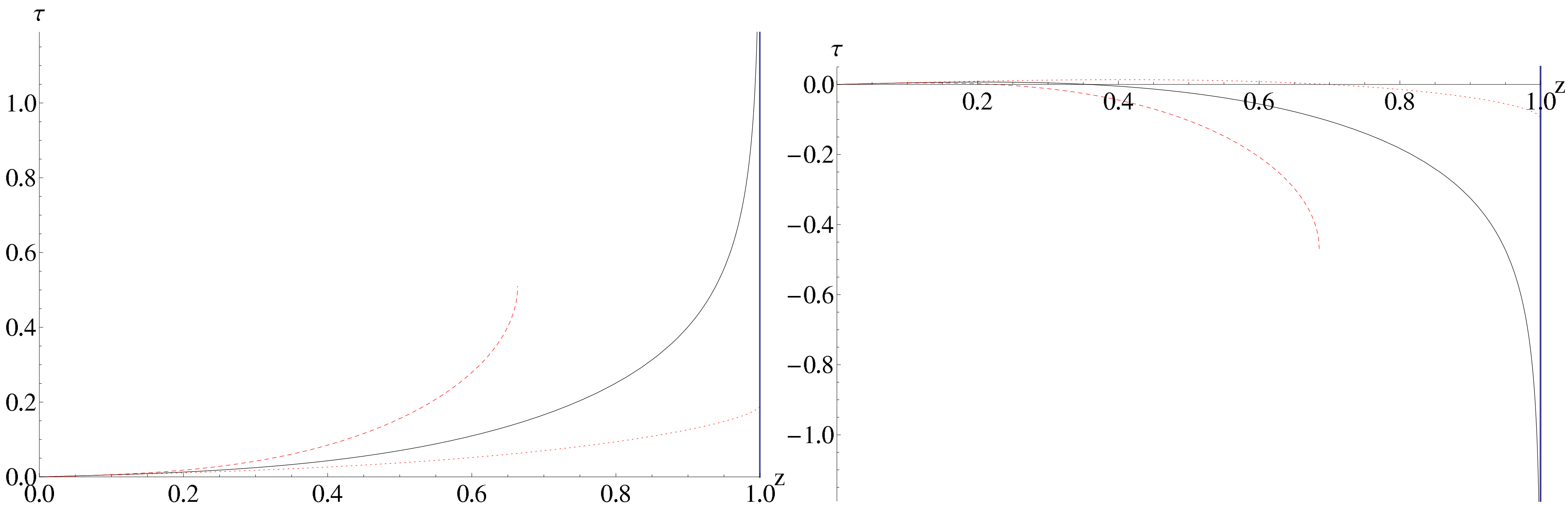

All the graphs are plotted using $z_\Lambda = 1$, $\mu^2 = \pi$ and $c_1 = 0.05$. The tip of the cigar is at $z = z_\Lambda = 1$. On the left, the solid black line represents a solution with $c_3 \approx 0.3579$ for which τ diverges at z_Λ. The red dashed line has a too large c_3 ($c_3 = 1$) - such that there is a singularity at $z = z_s$ where $\partial_z \tau$ diverges while τ stays finite. This is unacceptable since the solution stops at $z = z_s$ where the energy density of the flavor branes diverges. The red dotted line corresponds to $c_3 = 0.1$; this kind of solution is discarded because the tachyon stays finite everywhere. The plot in the right is done with the same conventions but with negative values of $c_3 = -0.1, -0.3893, -1$. For $c_3 \approx -0.3893$ there is a solution of the differential equation such that τ diverges to $-\infty$. This solution is unstable.

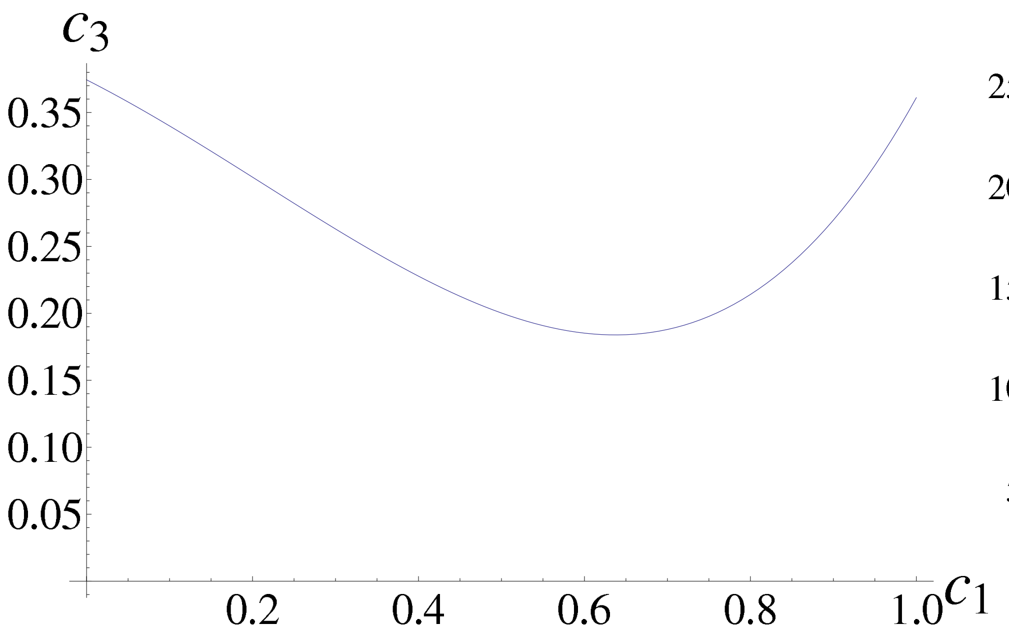

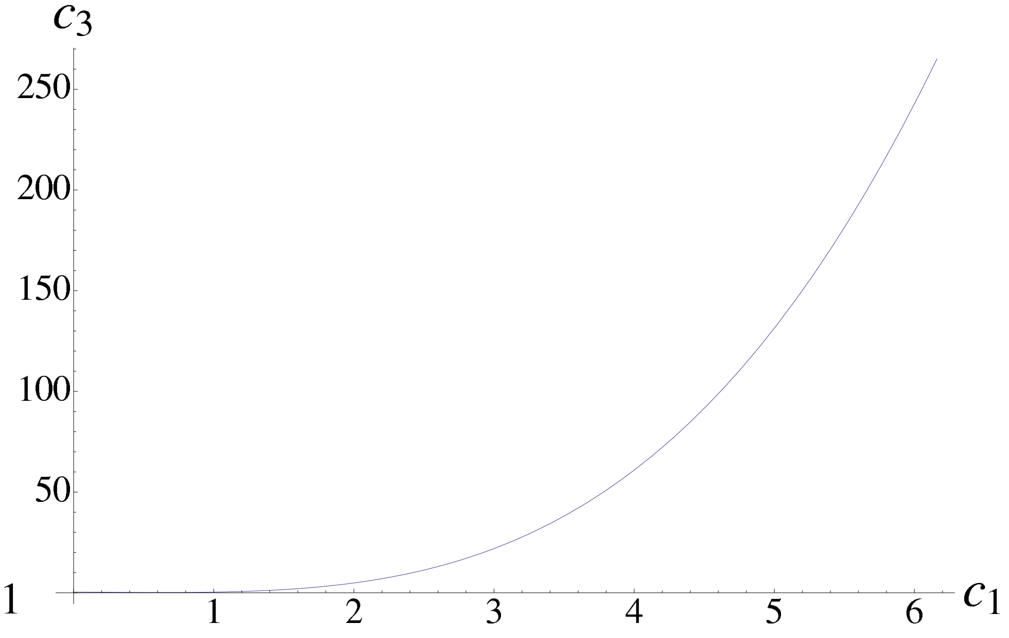

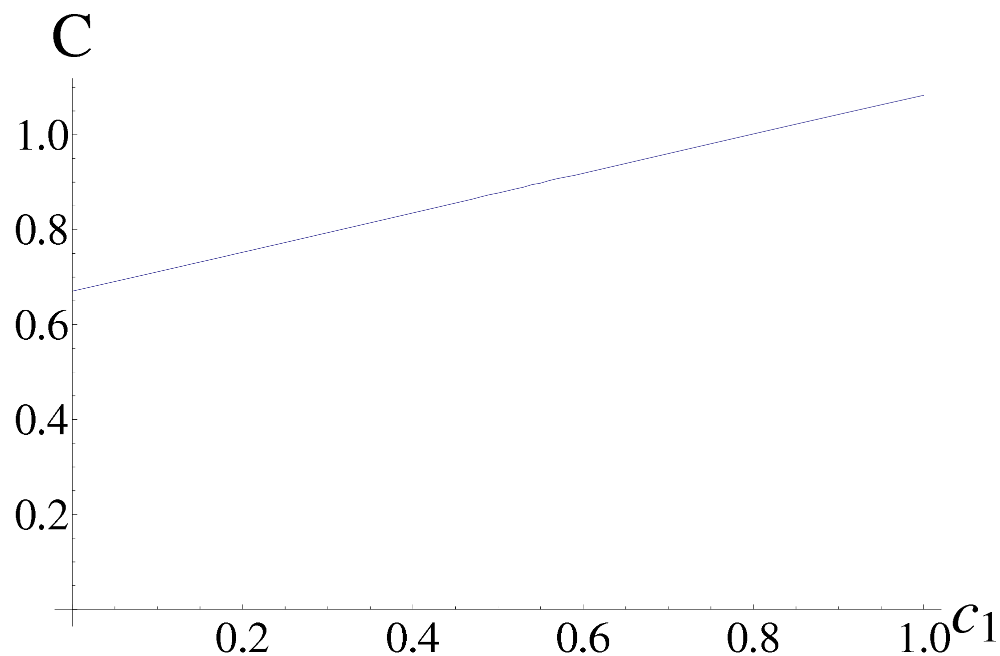

- Chiral symmetry breaking is manifest.

Chiral restauration at deconfinement

• In the deconfined phase, the bulk metric is that of a bh, and the tachyon equation becomes

$$\tau'' + \frac{\mu^2 z^2 f_T}{3}\tau'^3\left(-\frac{4}{z}+\frac{f_T'}{2f_T}\right)+\left(-\frac{3}{z}+\frac{f_T'}{f_T}\right)\tau' + \left(\frac{3}{z^2 f_T}+\mu^2\tau'^2\right)\tau = 0$$

• The branes now are allowed to enter the horizon without recombining.

• To avoid intermediate singularities of the solution the boundary conditions must be tuned so that tachyon is finite at the horizon.

• Near the horizon the correct solution behaves as a one-parameter family

$$\tau = c_T - \frac{3c_T}{5z_T}(z_T - z) - \frac{9c_T}{200z_T}(8+\mu^2 {c_T}^2)(z_T-z)^2 + \ldots$$

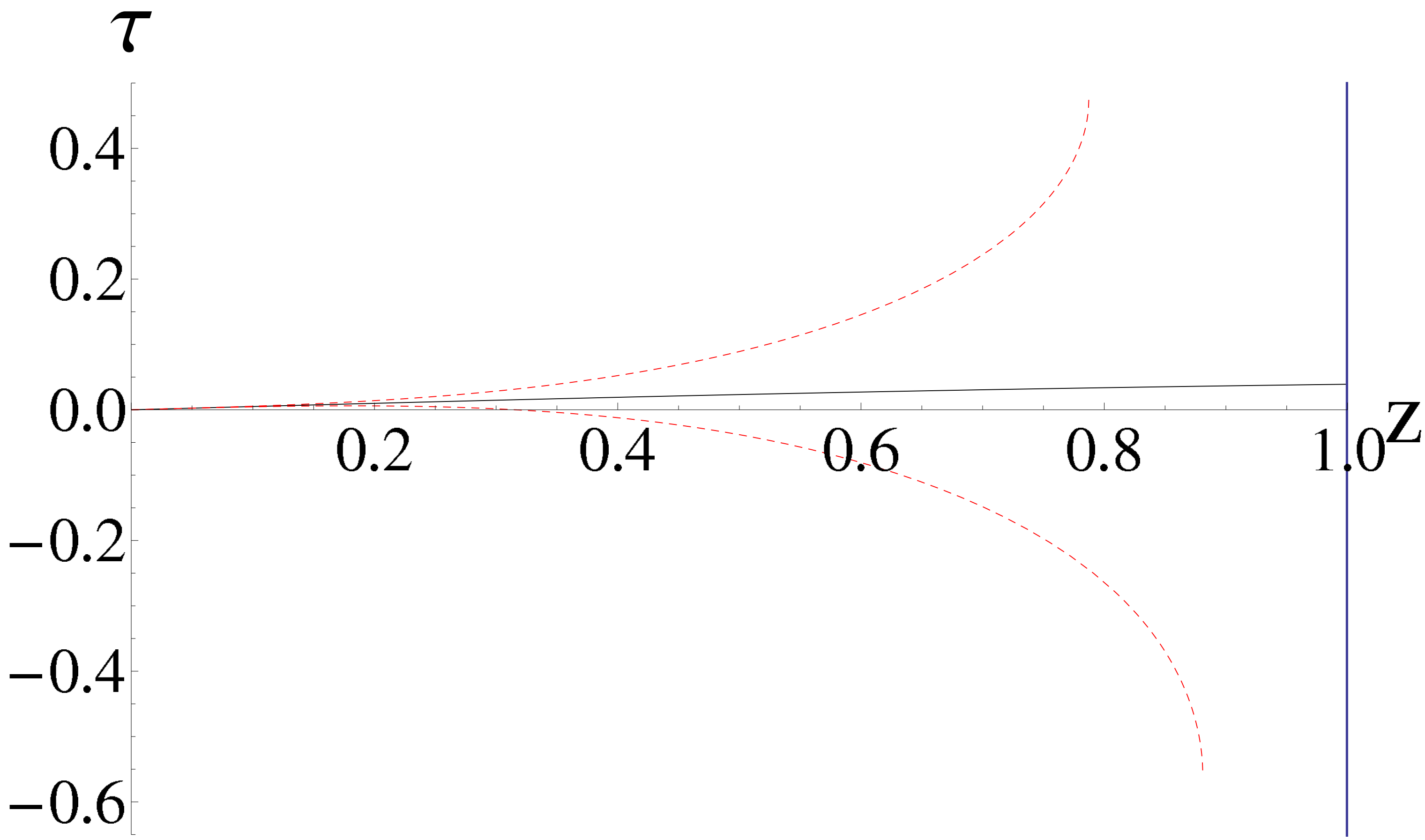

Plots corresponding to the deconfined phase. We have taken $c_1 = 0.05$. The solid line displays the physical solution $c_3 = -0.0143$ whereas the dashed lines ($c_3 = -0.5$ and $c_3 = 0.5$) are unphysical and end with a behavior of the type $\tau = k_1 - k_2\sqrt{z_s - z}$.

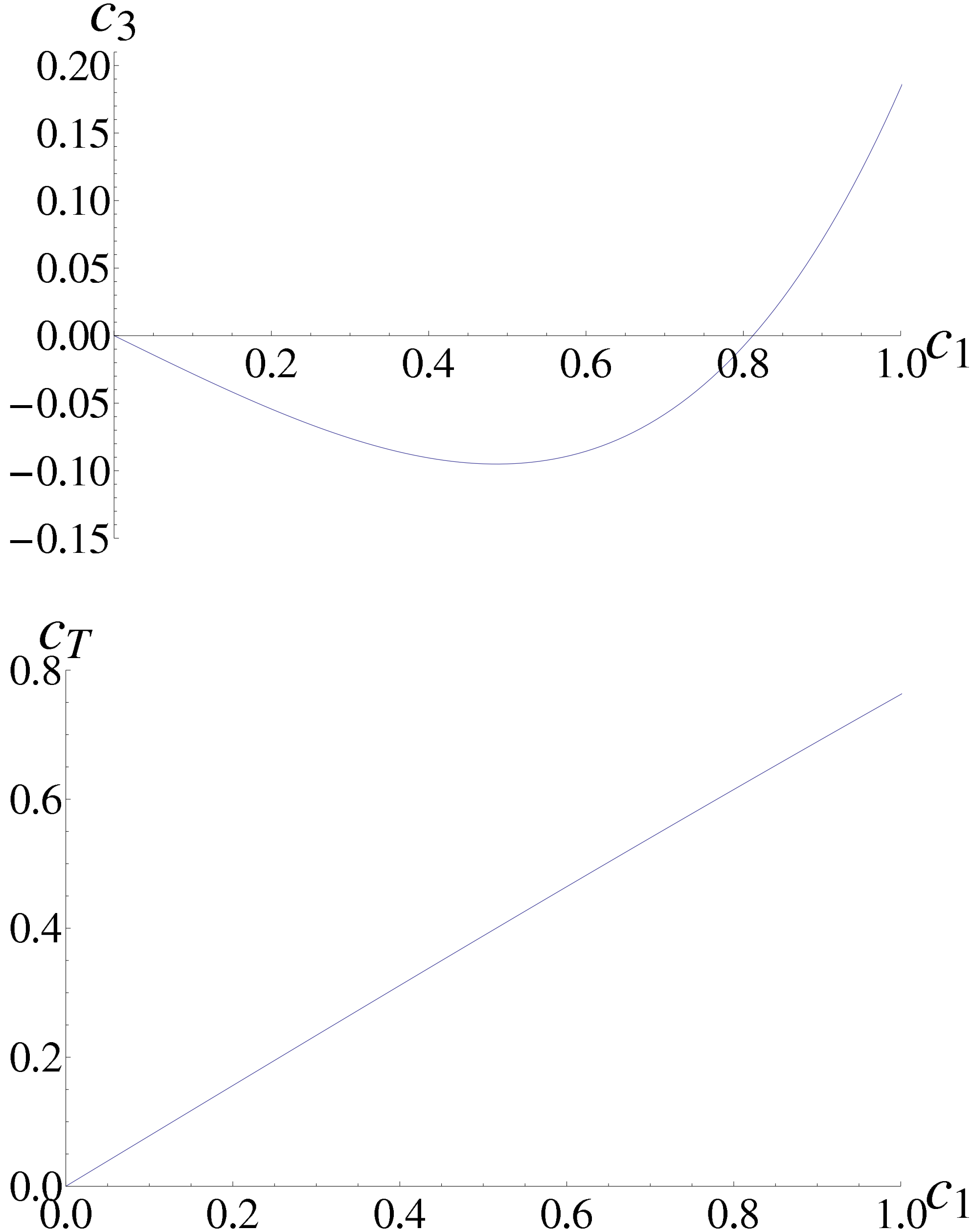

These plots give the values of c_3 and c_T determined numerically by demanding the correct IR behavior of the solution, as a function of c_1.

Jump of the condensate at the phase transition

• From holographic renormalization we obtain

$$\langle \bar{q}q \rangle = \frac{1}{\beta}(2\pi\alpha' \mathcal{K} R^3 \lambda)\left(-4c_3 + \left(\frac{m_q}{\beta}\right)^3 \mu^2(1+\alpha)\right) \quad , \quad m_q = \beta\ c_1$$

• We calculate the jump at the phase transition that is scheme independent for a fixed quark mass.

$$\Delta\langle \bar{q}q \rangle \equiv \langle \bar{q}q \rangle_{conf} - \langle \bar{q}q \rangle_{deconf} = -4\frac{1}{\beta}(2\pi\alpha' \mathcal{K} R^3 \lambda)\Delta c_3$$

• This is equivalent to Δc_3

• We plot it as a function of the quark mass.

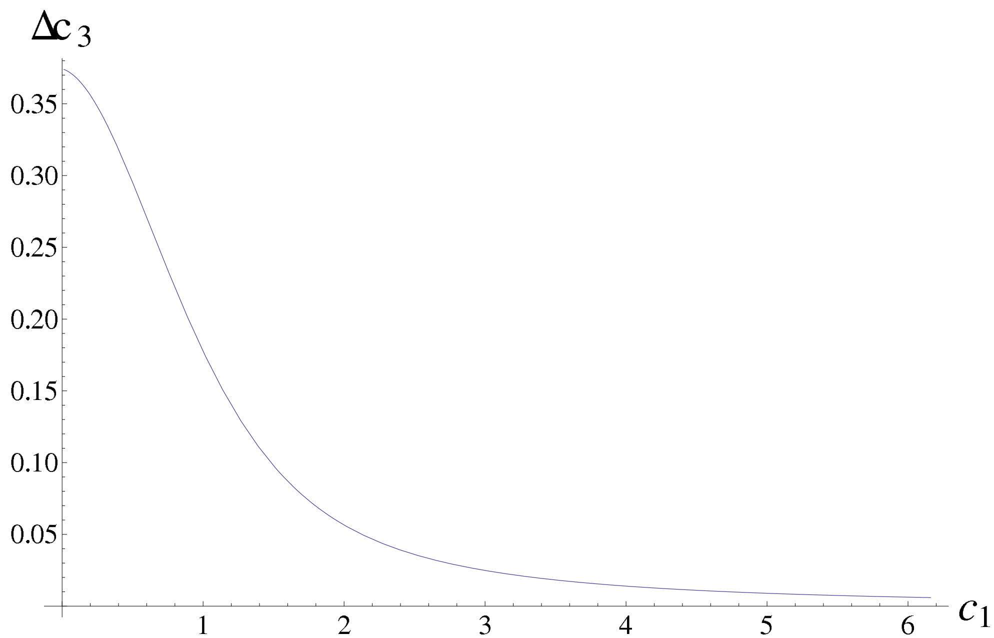

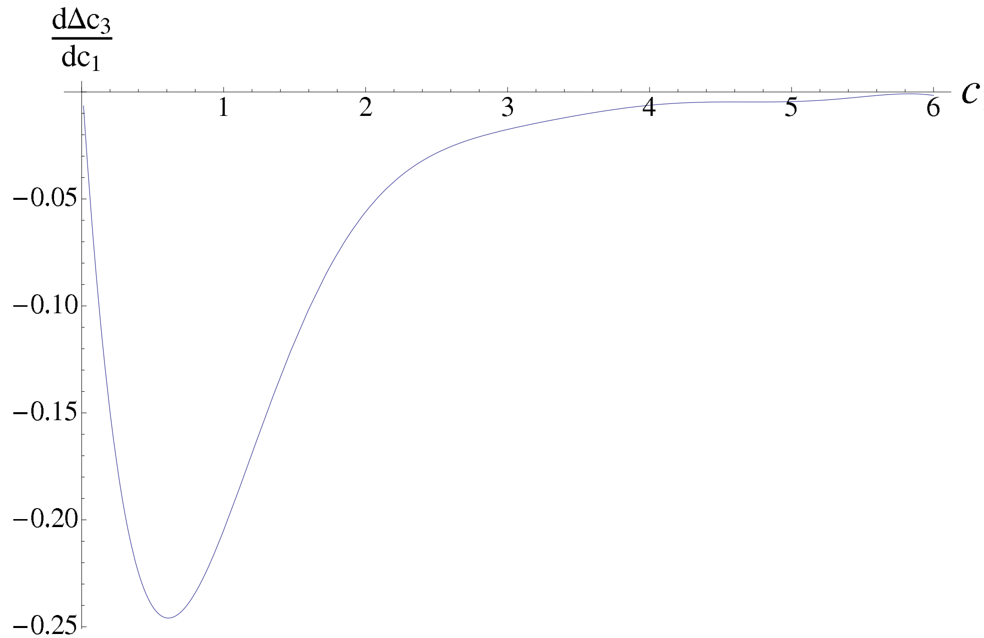

The finite jump of the quark condensate and its derivative with respect to c_1 when the confinement-deconfinement transition takes place. The important features appear when $m_q \sim \Lambda_{QCD}$

- Another interesting quantity is

$$\langle\bar{q}q\rangle_R = \frac{m_q}{T_c^4}(\langle\bar{q}q\rangle_T - \langle\bar{q}q\rangle_0) \approx N_c\frac{m_q}{T_c^4}(0.3\beta T_c^3 + 0.09 m_q T^2)\ , \qquad (T > T_c)$$

that tracks the T-dependence of the condensate.

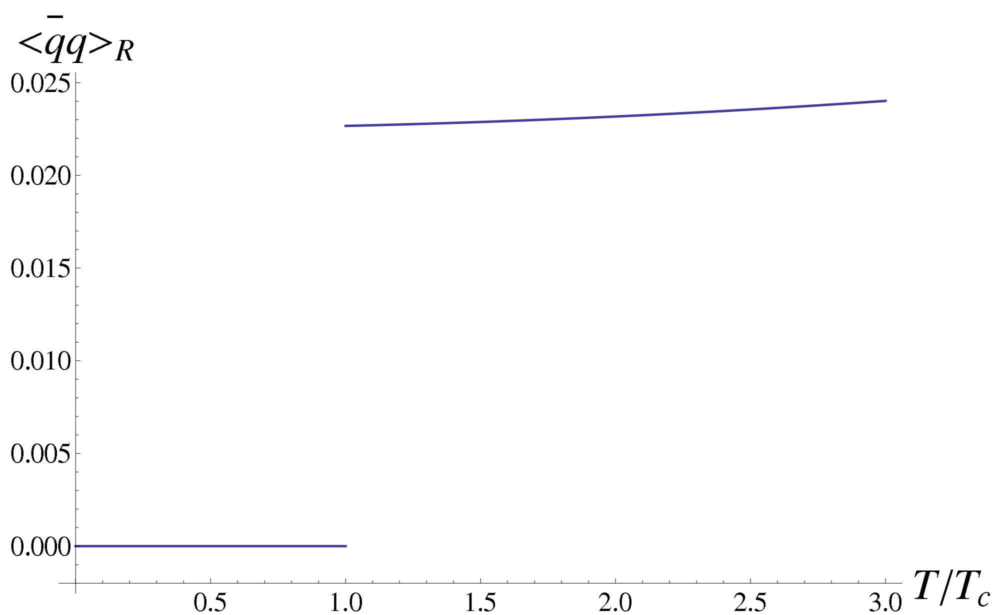

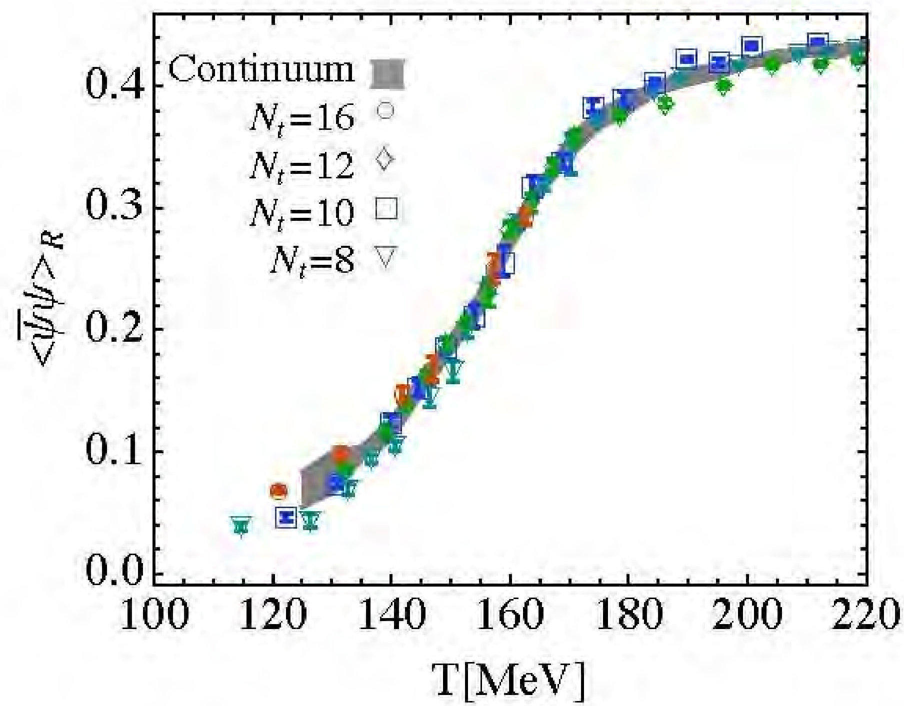

We have taken $\beta = 1$, $m_q/T_c = 1/40$ for the plot.

S. Borsanyi, Z. Fodor, C. Hoelbling, S. D. Katz, S. Krieg, C. Ratti, K. K. Szabo [Wuppertal-Budapest Collaboration], [ArXiv:1005.3508][hep-lat].

Meson spectra

For the vectors

$$z_\Lambda m_V^{(1)} = 1.45 + 0.718 c_1 \,, \qquad z_\Lambda m_V^{(2)} = 2.64 + 0.594 c_1 \,, \qquad z_\Lambda m_V^{(3)} = 3.45 + 0.581 c_1 \,,$$
$$z_\Lambda m_V^{(4)} = 4.13 + 0.578 c_1 \,, \qquad z_\Lambda m_V^{(5)} = 4.72 + 0.577 c_1 \,, \qquad z_\Lambda m_V^{(6)} = 5.25 + 0.576 c_1 \,.$$

For the axial vectors:

$$z_\Lambda m_A^{(1)} \approx 2.05 + 1.46 c_1 \,, \qquad z_\Lambda m_A^{(2)} \approx 3.47 + 1.24 c_1 \,, \qquad z_\Lambda m_A^{(3)} \approx 4.54 + 1.17 c_1 \,,$$
$$z_\Lambda m_A^{(4)} \approx 5.44 + 1.13 c_1 \,, \qquad z_\Lambda m_A^{(5)} \approx 6.23 + 1.11 c_1 \,, \qquad z_\Lambda m_A^{(6)} \approx 6.95 + 1.10 c_1 \,.$$

For the pseudoscalars:

$$z_\Lambda m_P^{(1)} \approx \sqrt{3.53 c_1^2 + 6.33 c_1} \,, \qquad z_\Lambda m_P^{(2)} \approx 2.91 + 1.40 c_1 \,, \qquad z_\Lambda m_P^{(3)} \approx 4.07 + 1.27 c_1 \,,$$
$$z_\Lambda m_P^{(4)} \approx 5.04 + 1.21 c_1 \,, \qquad z_\Lambda m_P^{(5)} \approx 5.87 + 1.17 c_1 \,, \qquad z_\Lambda m_P^{(6)} \approx 6.62 + 1.15 c_1 \,.$$

For the scalars:

$$z_\Lambda m_S^{(1)} = 2.47 + 0.683 c_1 \,, \qquad z_\Lambda m_S^{(2)} = 3.73 + 0.488 c_1 \,, \qquad z_\Lambda m_S^{(3)} = 4.41 + 0.507 c_1 \,,$$
$$z_\Lambda m_S^{(4)} = 4.99 + 0.519 c_1 \,, \qquad z_\Lambda m_S^{(5)} = 5.50 + 0.536 c_1 \,, \qquad z_\Lambda m_S^{(6)} = 5.98 + 0.543 c_1 \,.$$

- Valid up to $c_1 \sim 1$. For the axials and pseudo-scalars, we used $k = \frac{18}{\pi^2}$.
- In qualitative agreement with lattice results
  Laerman+Schmidt., Del Debbio+Lucini+Patela+Pica, Bali+Bursa

- The GOR relation is satisfied

$$-4m_q\langle q\bar{q}\rangle = m_\pi^2 f_\pi^2$$

- The vector two-point function has the appropriate form

$$\int d^4x\, e^{iqx}\langle J_\mu(x)J_\nu(0)\rangle = (\eta_{\mu\nu}q^2 - q^\mu q^\nu)\Pi_V(q^2)$$

$$\Pi_V = -\frac{N_c}{12\pi^2}\left[\log\frac{q^2}{z_\Lambda^2} - 1 - \log 4 + 2\gamma - 9\frac{z_\Lambda^4}{q^4} + \cdots\right]$$

- Decay widths can be calculated from the wave-functions

$$F_n^2 = \frac{N_c}{6\pi^2}\frac{R}{m_n^2}\left(\left.\frac{d^2\psi_V^{(n)}}{dz^2}\right|_{z=0}\right)^2$$

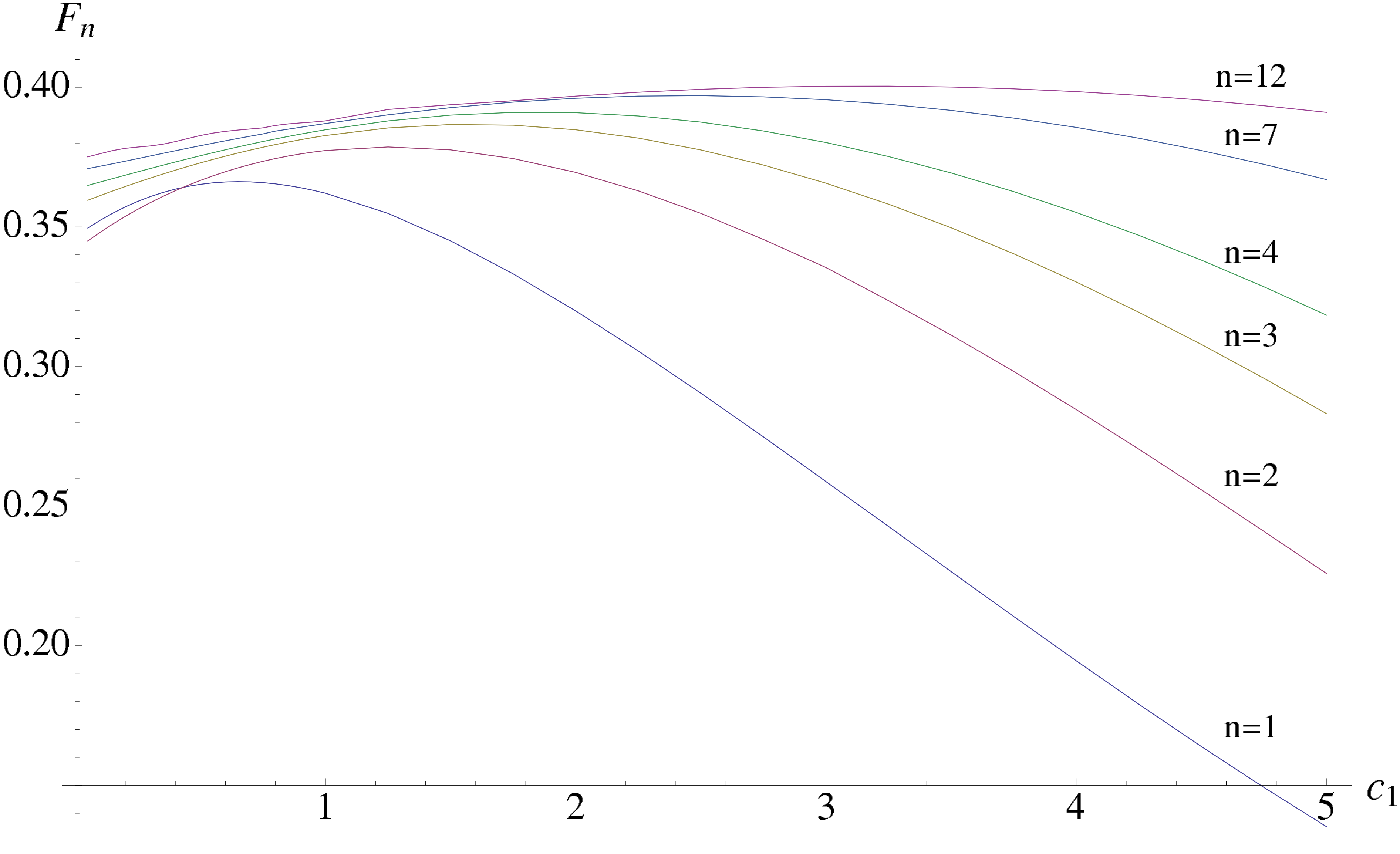

The decay constant, in units of z_Λ^{-1} for the four lowest-lying, the seventh and the twelve-th vector mode (from bottom to top), as a function of c_1. The numerical plot was made by taking $\mu^2 = \pi$ and $N_c = 3$.

Mass dependence of f_π

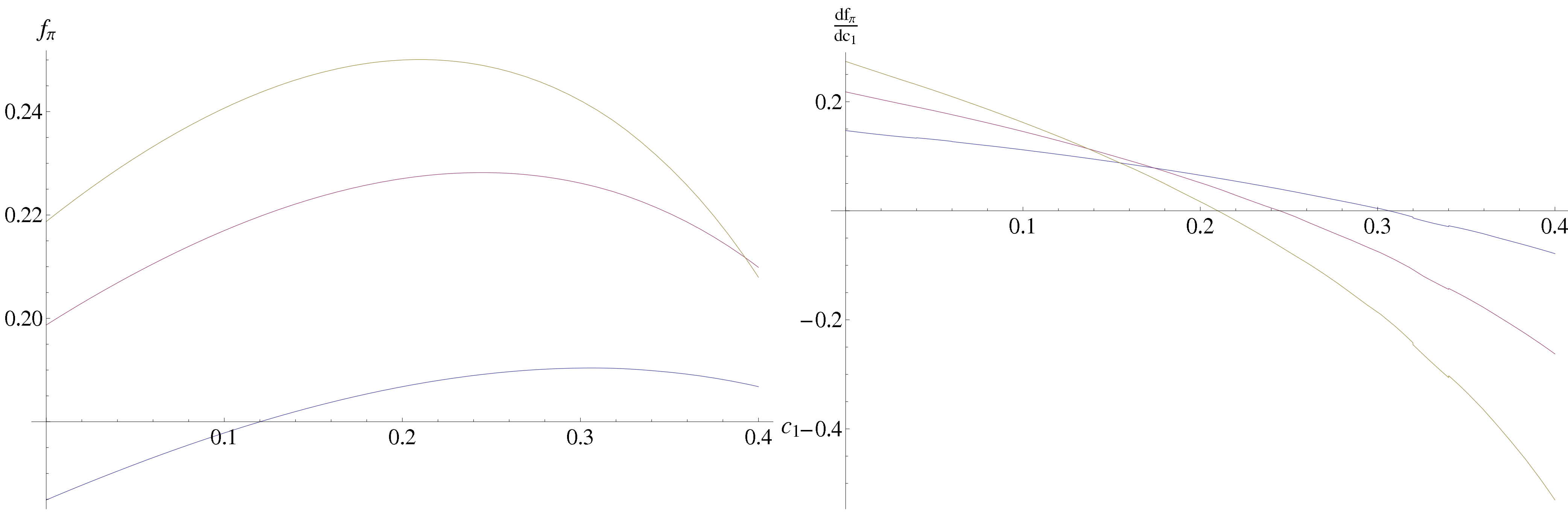

The pion decay constant and its derivative as a function of c_1 - the quark mass. The different lines correspond to different values of k. From bottom to top (on the right plot, from bottom to top in the vertical axis) $k = \frac{12}{\pi^2}, \frac{24}{\pi^2}, \frac{36}{\pi^2}$. The pion decay constant comes in units of z_Λ^{-1}.

Linear Regge Trajectories

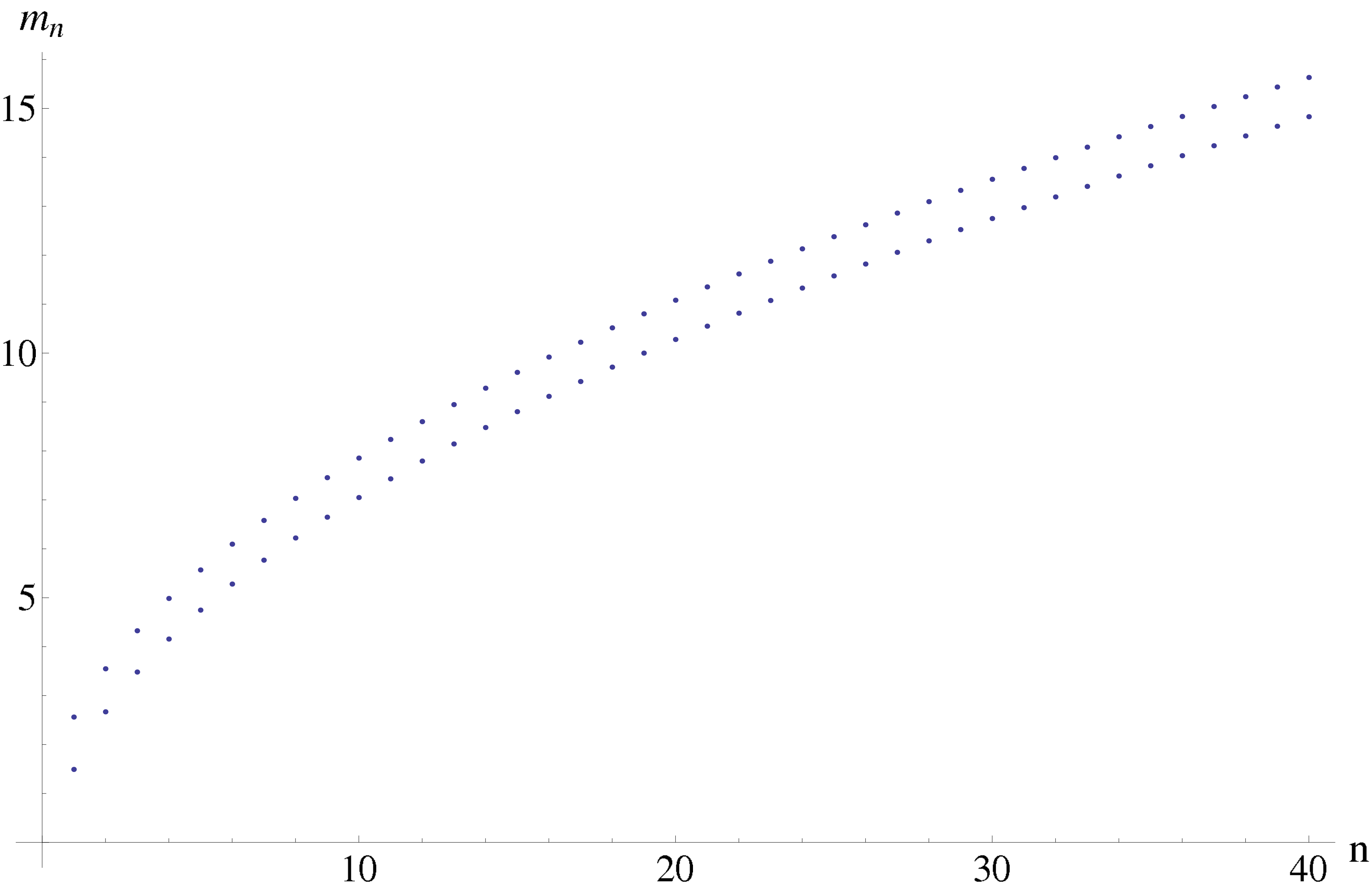

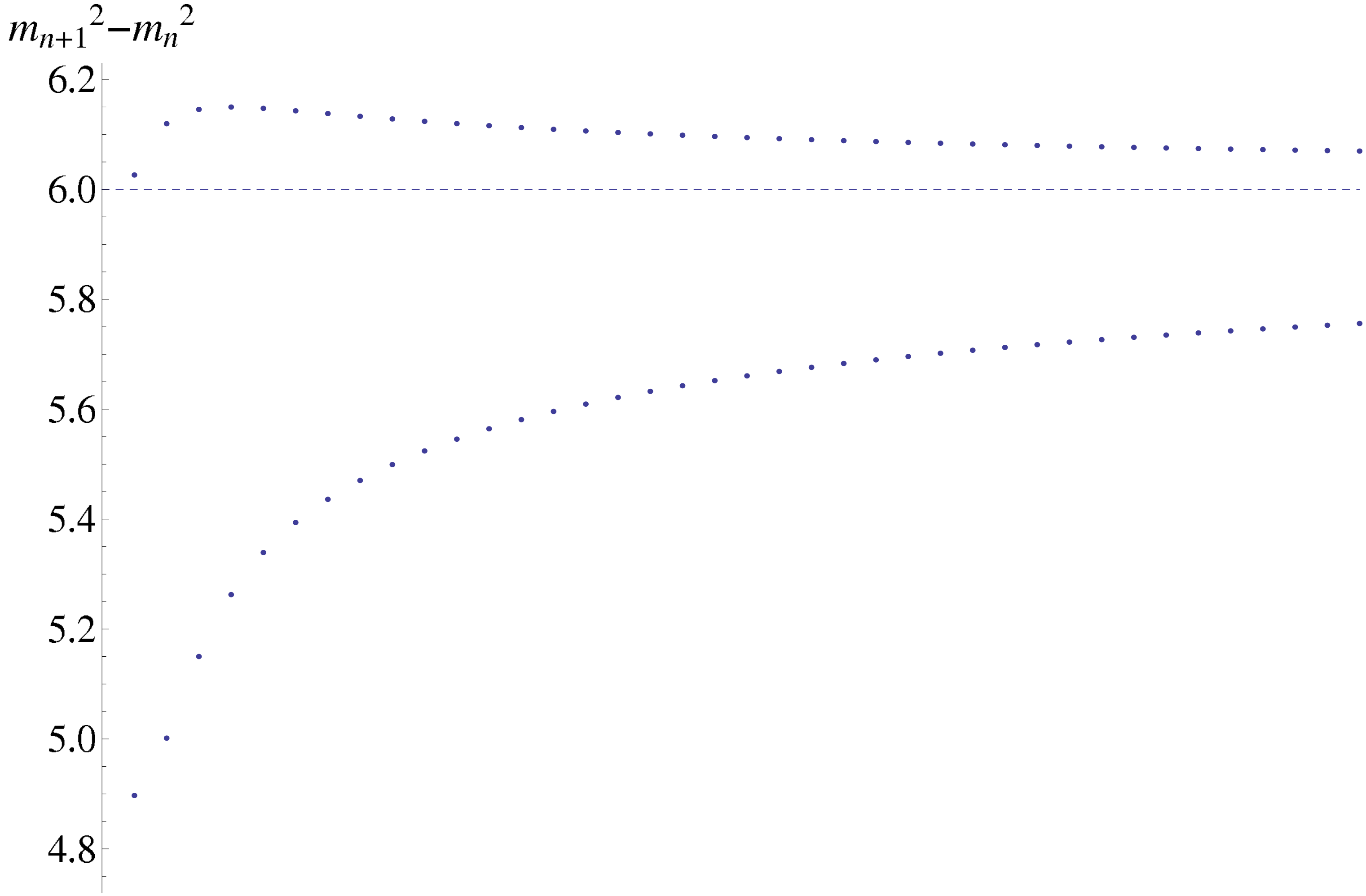

Results corresponding to the forty lightest vector states with $c_1 = 0.05$ and $c_1 = 1.5$. On the right, the horizontal line signals the asymptotic value 6 of the Regge trajectory, the lower line corresponds to $c_1 = 0.05$ and the upper line to $c_1 = 1.5$. Masses are given in units of z_Λ^{-1}. $m_{n+1}^2 - m_n^2 = \frac{6}{z_\Lambda^2} + \mathcal{O}(1/n)$.

Fit to data

We fit the three parameters to the “confirmed” isospin 1 mesons

$$z_\Lambda^{-1} = 549\ MeV \quad , \quad c_{1l} z_\Lambda = 0.0094 \quad , \quad k = \frac{18}{\pi^2}$$

minimizing

$$\epsilon_{rms} = \left(\frac{1}{n} \sum_i \left(\frac{\delta O_i}{O_i} \right)^2 \right)^{\frac{1}{2}}$$

where n is the number of the observables minus the number of the fitted parameters, $n = 9 - 3$. The rms error then is $\epsilon_{rms} = 14.5\%$

- For masses

J^{CP}	Meson	Measured (MeV)	Model (MeV)	$100\|\delta O\|/O$
1^{--}	$\rho(770)$	775	800	3.2%
	$\rho(1450)$	1465	1449	1.1%
1^{++}	$a_1(1260)$	1230	1135	7.8%
0^{-+}	π_0	135.0	134.2	0.5%
	$\pi(1300)$	1300	1603	23.2%
0^{++}	$a_0(1450)$	1474	1360	7.7%

- For decay constants

J^{CP}	Meson	Measured (MeV)	Model (MeV)	$100\|\delta O\|/O$
1^{--}	$\rho(770)$	216	190	12%
1^{++}	$a_1(1260)$	216	228.5	5.8%
0^{-+}	π_0	127	101.3	20.2%

- Masses of "less confirmed mesons"

J^{PC}	Meson	Measured (MeV)	Model (MeV)
1^{--}	$\rho(2270)$	2270	2649
1^{++}	$a_1(1930)$	1930	2166
	$a_1(2096)$	2096	2591
	$a_1(2270)$	2270	2965
	$a_1(2340)$	2340	3303
0^{-+}	$\pi(2070)$	2070	2406
	$\pi(2360)$	2360	2798
0^{++}	$a_0(2020)$	2025	1883

- The RMS error here is 23%. Axial vector mesons are consistently over-estimated.

"$s\bar{s}$" states

They can be "estimated" using

$$m(\text{"}\eta\text{"}) = \sqrt{2m_K^2 - m_\pi^2} \quad , \quad m(\text{"}\phi(1020)\text{"}) = 2m(K^*(892)) - m(\rho(770)) \quad , \quad .$$

Allton+Gimenez+Giusti+Rapuano

J^{PC}	Meson	"Measured" (MeV)	Model (MeV)
1^{--}	"$\phi(1020)$"	1009	857
	"$\phi(1680)$"	1363	1432
1^{++}	"$f_1(1420)$"	1440	1188
0^{-+}	"η"	691	740
	"$\eta(1475)$"	1620	1608
0^{++}	"$f_0(1710)$"	1386	1365

The "mass" of the s-quark is $c_{1,s} = 0.350$. The rms error for this set of observables ($n = 6 - 1$) is $\varepsilon_{rms} = 11\%$.

- $\frac{2m_s}{m_u+m_d} \simeq \frac{c_{1,s}}{c_{1,l}} \simeq 26$

- $T_{deconf} = \frac{5}{4\pi z_\Lambda} \simeq 215 MeV$.

Steps forward

Advantages of this simple AdS/QCD-like model

• Compared to the SS model it contains all trajectories corresponding to $1^{--}, 1^{++}, 0^{-+}, 0^{++}$ and can accommodate a mass of the quarks. The asymptotic masses of mesons are $m_n^2 \sim n$, as they should.

• Compared to the soft-wall AdS/QCD model:

(a) The background glue solution is a consistent solution with proper thermodynamics.

(b) The magnetic quarks are confined instead of screened.

(c) Chiral symmetry breaking is dynamical.

(d) The mass of the ρ meson depends on the quark (or pion) mass.

(e) The finite density physics is sensitive to quark masses.

Numerical solutions: $T = 0$

$T \equiv 0$ backgrounds (color codes λ, A)

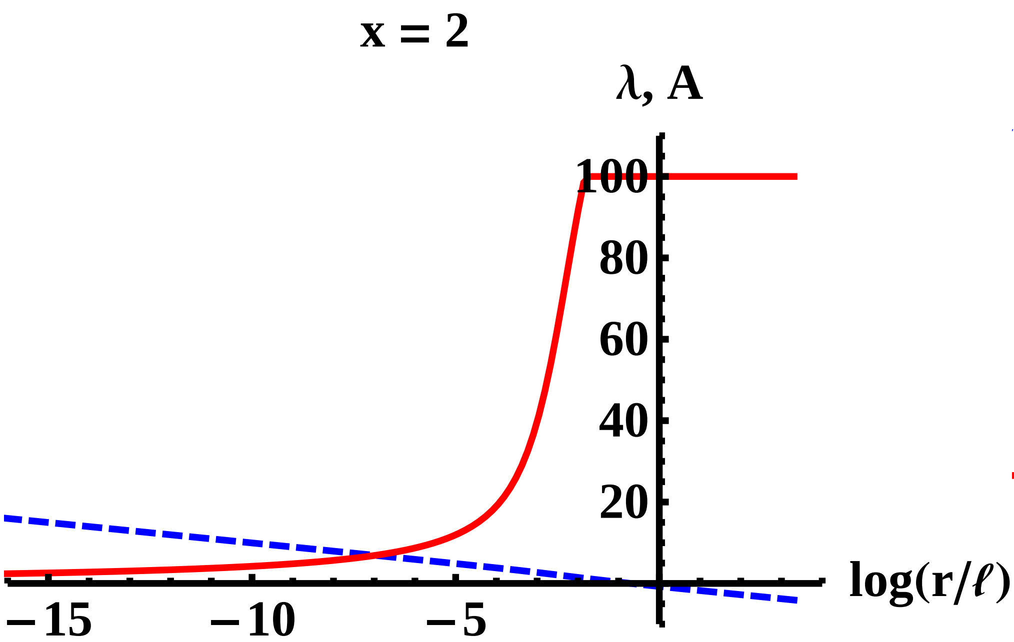

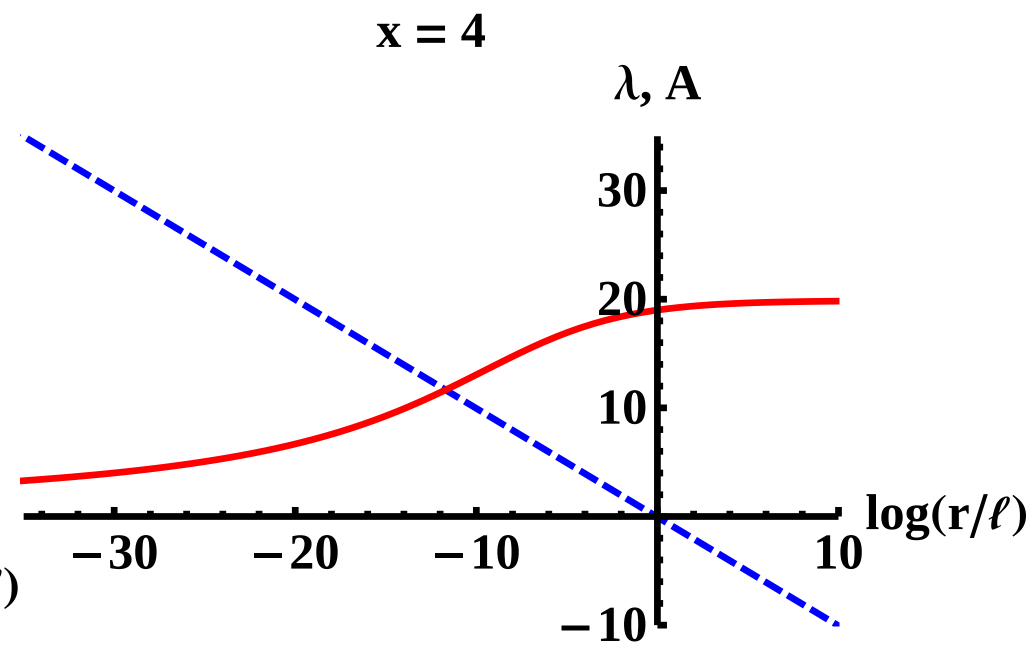

Numerical solutions: Massless with $x < x_c$

Massless backgrounds with $x < x_c \simeq 3.9959$ (λ, A, T)

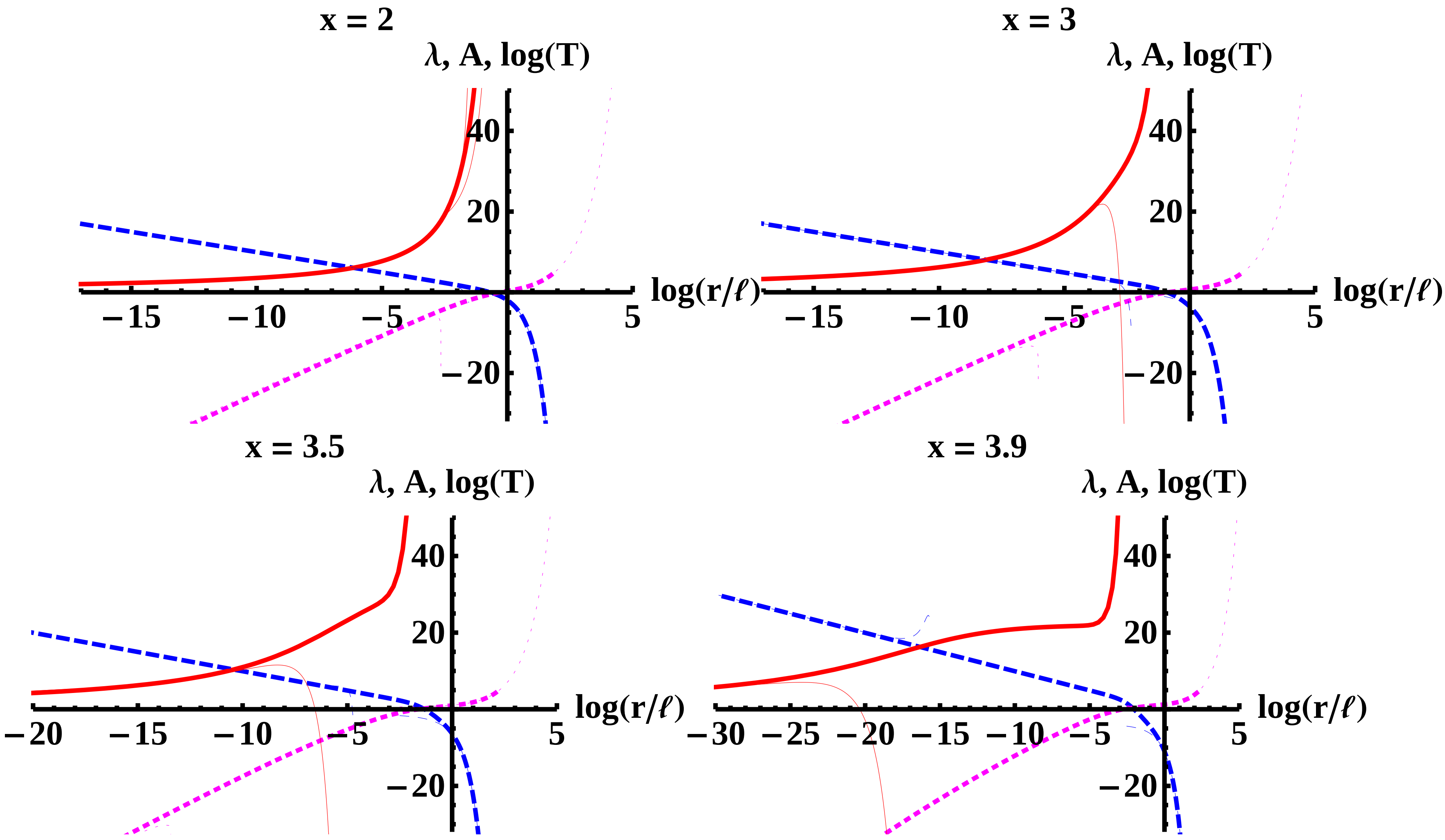

Massless backgrounds: beta functions $\beta = \frac{d\lambda}{dA}$, ($x_c \simeq 3.9959$)

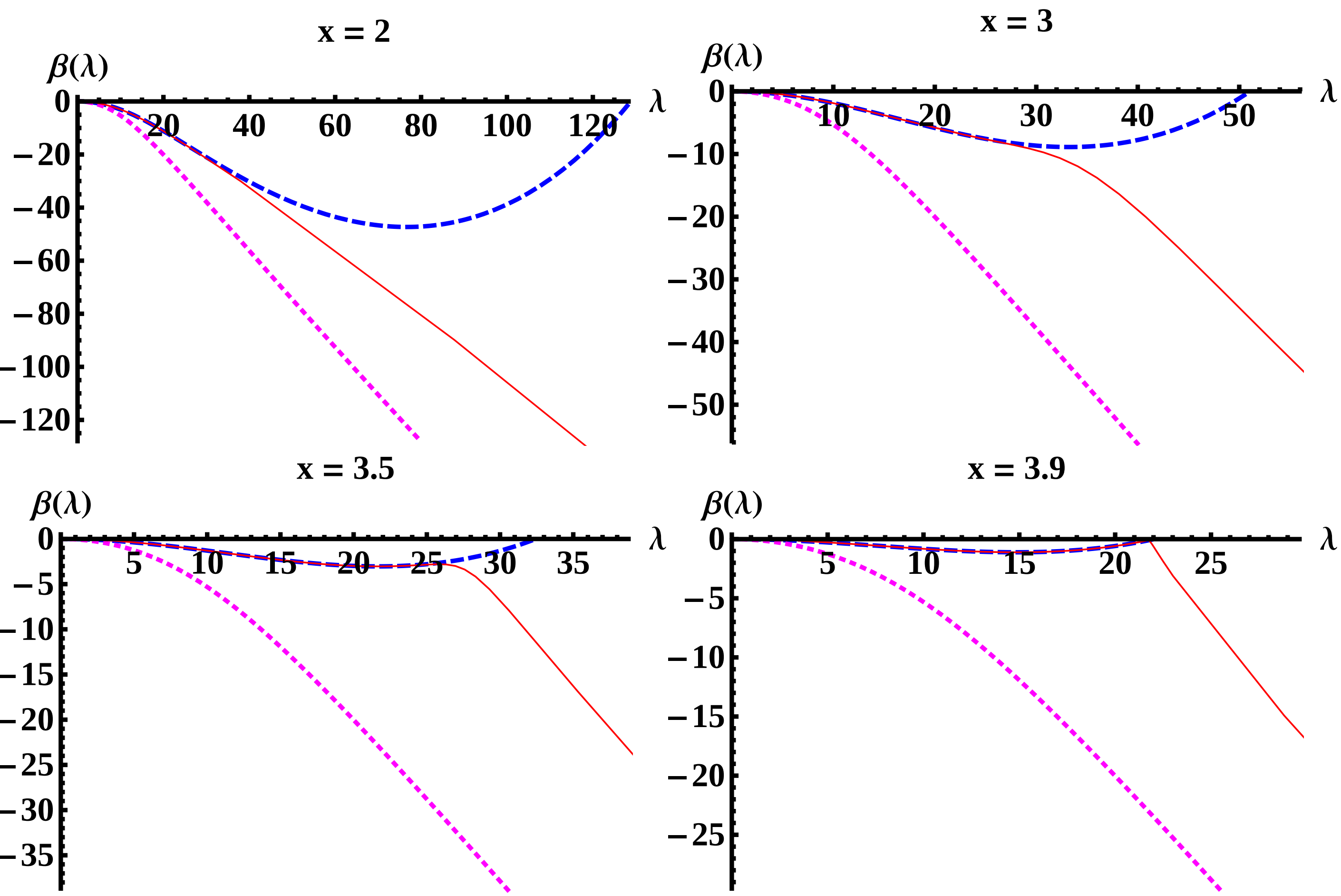

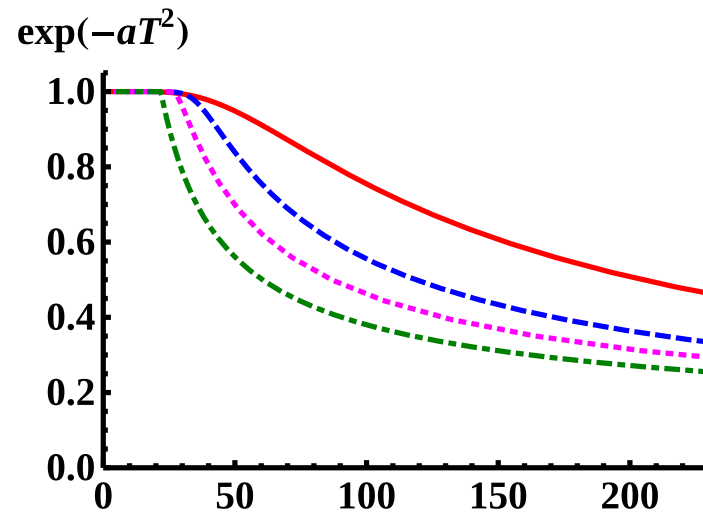

$x = 2, 3, 3.5, 3.9$

.

Massless backgrounds: gamma functions $\frac{\gamma}{T} = \frac{d \log T}{dA}$

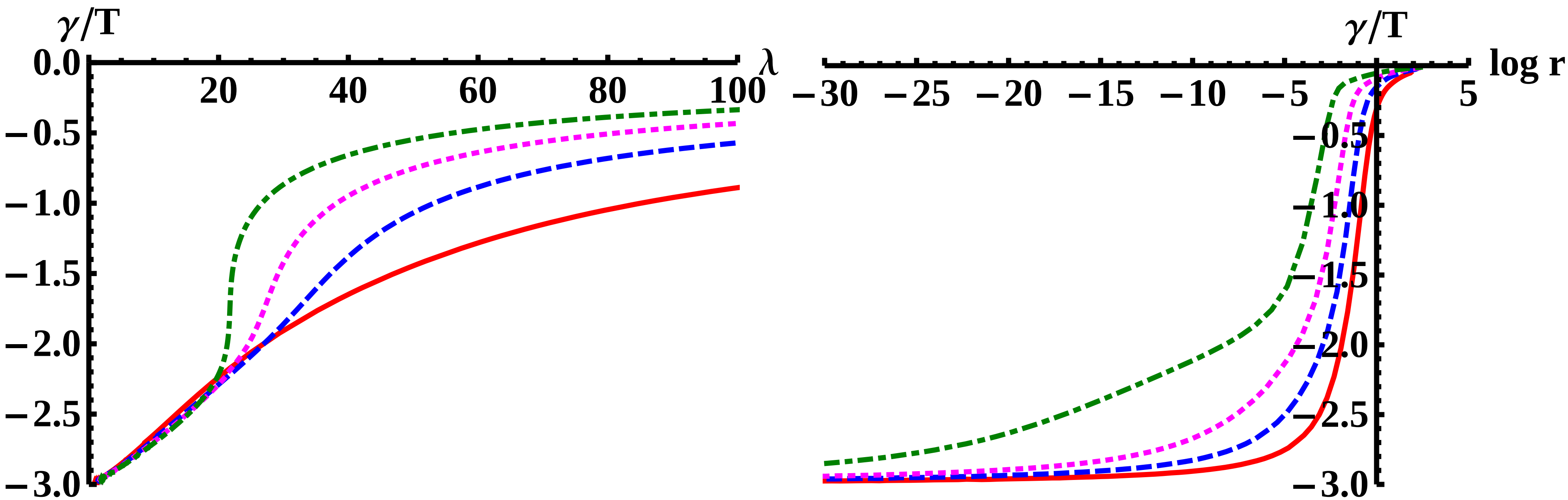

$x = 2, 3, 3.5, 3.9$

Comparison to N=1 sQCD

The case of $\mathcal{N} = 1$ $SU(N_c)$ superQCD with N_f quark multiplets is known and provides an interesting (and more complex) example for the non-supersymmetric case. From Seiberg we have learned that:

- $x = 0$ the theory has confinement, a mass gap and N_c distinct vacua associated with a spontaneous breaking of the leftover R symmetry Z_{N_c}.

- At $0 < x < 1$, the theory has a runaway ground state.

- At $x = 1$, the theory has a quantum moduli space with no singularity. This reflects confinement with χSB.

- At $x = 1 + \frac{1}{N_c}$, the moduli space is classical (and singular). The theory confines, but there is no χSB.

- At $1 + \frac{2}{N_c} < x < \frac{3}{2}$ the theory is in the non-abelian magnetic IR-free phase, with the magnetic gauge group $SU(N_f - N_c)$ IR free.

• At $\frac{3}{2} < x < 3$, the theory flows to a CFT in the IR. Near $x = 3$ this is the Banks-Zaks region where the original theory has an IR fixed point at weak coupling. Moving to lower values, the coupling of the IR $SU(N_c)$ gauge theory grows. However near $x = \frac{3}{2}$ the dual magnetic $SU(N_f - N_c)$ is in its Banks-Zaks region, and provides a weakly coupled description the IR fixed point theory.

• At $x > 3$, the theory is IR free.

There are similarities and important differences with QCD:

• sQCD contains scalars and this gives rise to an extended potential and moduli space that is responsible for most of differences.

• The chiral symmetry works differently.

• There is a similarity with the magnetic gauge group. Here it is generated by the axial and vector mesons that are massless in the conformal window. However, unlike sQCD here they are always weakly coupled in the IR because of the large N_c limit.

UV mass vs T_0 and r_1

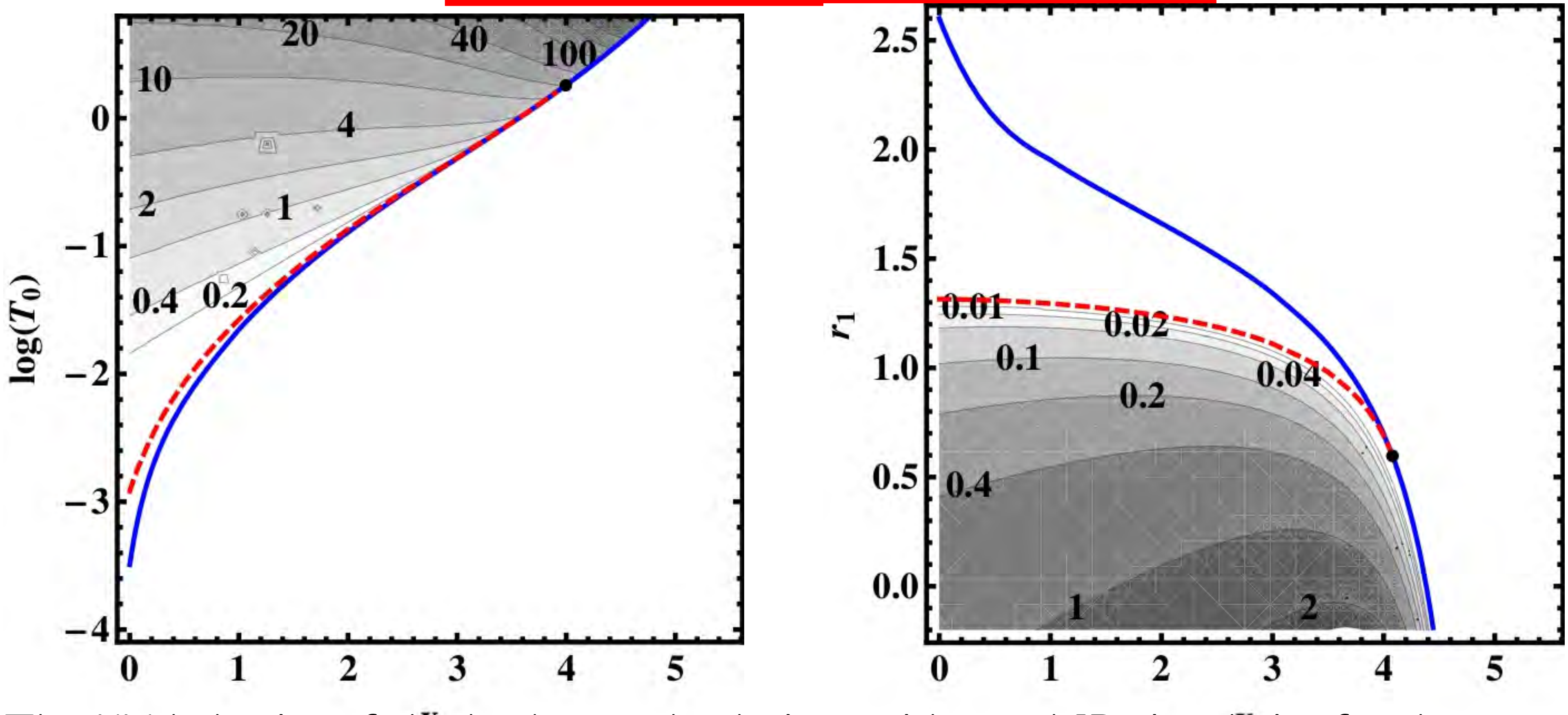

The UV behavior of the background solutions with good IR singularity for the scenario I (left) and parameter T_0 and scenario II (right) and parameter r_1.

The thick blue curve represents a change in the UV behavior, the red dashed curve has zero quark mass, and the contours give the quark mass. The black dot where the zero mass curve terminates lies at the critical value $x = x_c$. For scenario I (II) we have $x_c \simeq 3.9959$ ($x_c \simeq 4.0797$).

BKT scaling

We can derive

$$\Delta_{\rm IR}(4-\Delta_{\rm IR}) = -m_{\rm IR}^2 \ell_{\rm IR}^2 = G(\lambda_*, x) \ ,$$

where

$$G(\lambda, x) \equiv \frac{24 a(\lambda)}{h(\lambda)(V_g(\lambda) - x V_{f0}(\lambda))} \ .$$

and by matching behaviors

$$\sigma \sim \frac{1}{r_{\rm UV}^3} \exp\left(-\frac{2K}{\sqrt{\lambda_* - \lambda_c}}\right) \sim \frac{1}{r_{\rm UV}^3} \exp\left(-\frac{2\hat{K}}{\sqrt{x_c - x}}\right) \ .$$

x_c and λ_c are defined by $G(\lambda_*(x_c), x_c) = 4$ and $G(\lambda_c, x) = 4$, respectively, so that $\lambda_* = \lambda_c$ at $x = x_c$. we obtain

$$K = \frac{\pi}{\sqrt{\frac{\partial}{\partial \lambda} G(\lambda_c, x)}} \ ; \qquad \hat{K} = \frac{\pi}{\sqrt{-\frac{d}{dx} G(\lambda_*(x), x)\Big|_{x=x_c}}} \ .$$

.

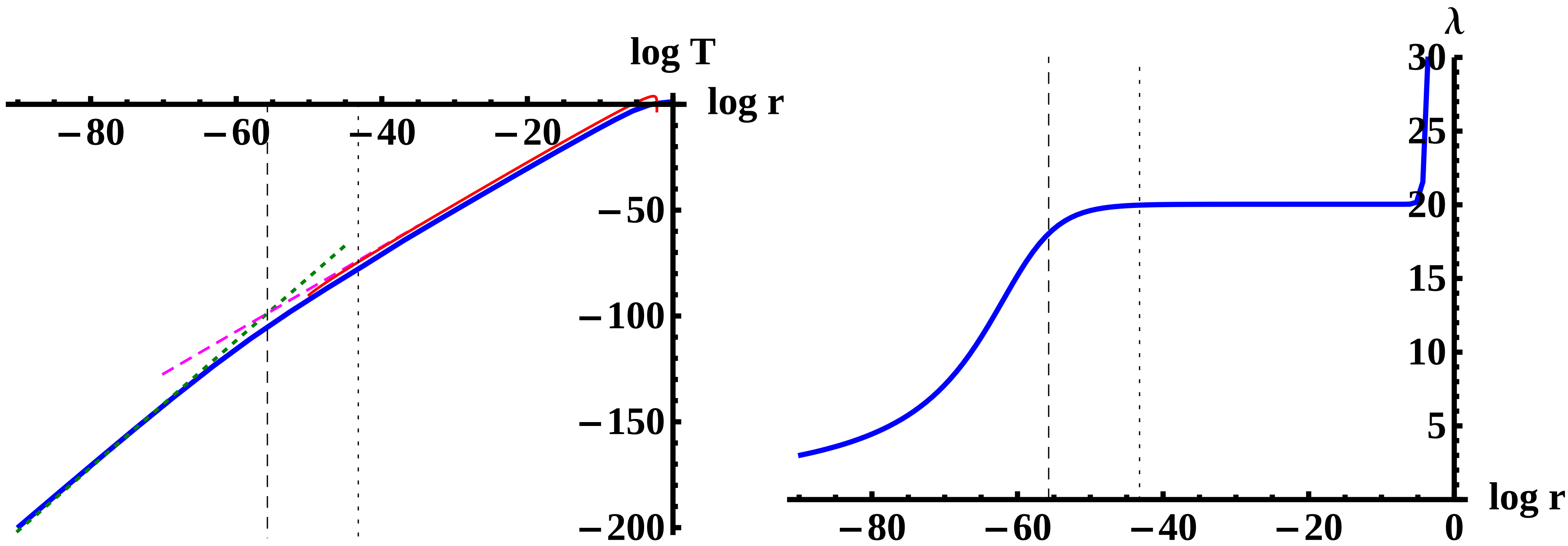

The tachyon $\log T$ (left) and the coupling λ (right) as functions of $\log r$ for an extreme walking background with $x = 3.992$. The thin lines on the left hand plot are the approximations used to derive the BKT scaling.

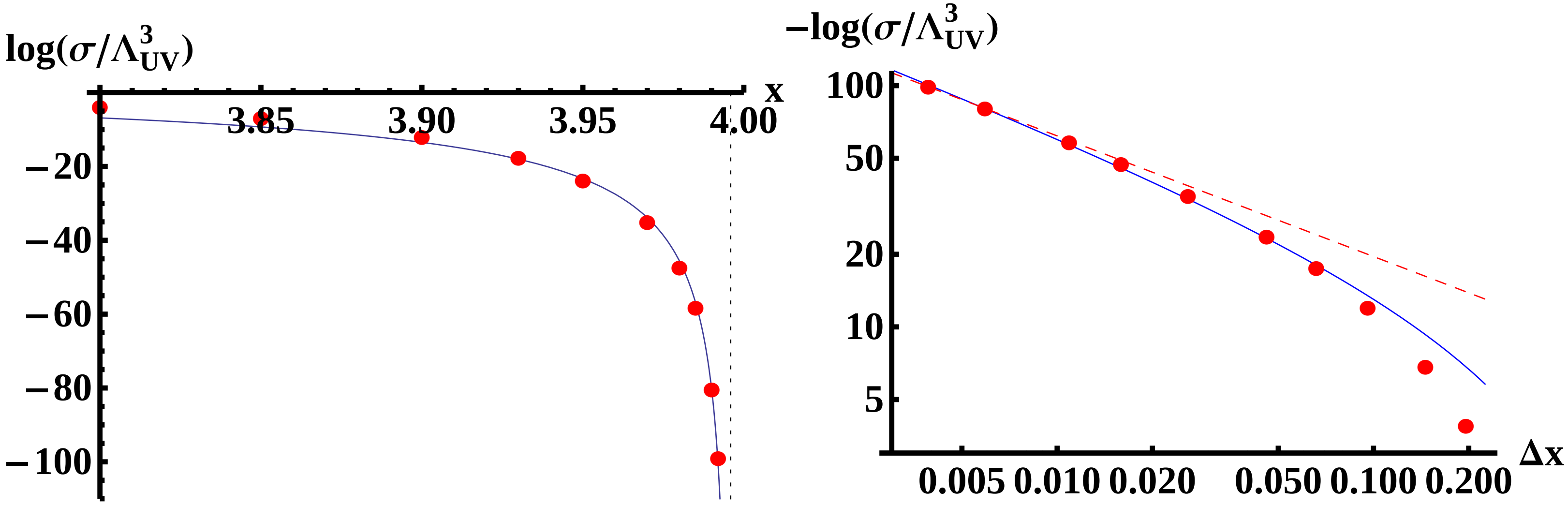

Left: $\log(\sigma/\Lambda^3)$ as a function of x (dots), compared to a BKT scaling fit (solid line). The vertical dotted line lies at $x = x_c$. Right: the same curve on log-log scale, using $\Delta x = x_c - x$.

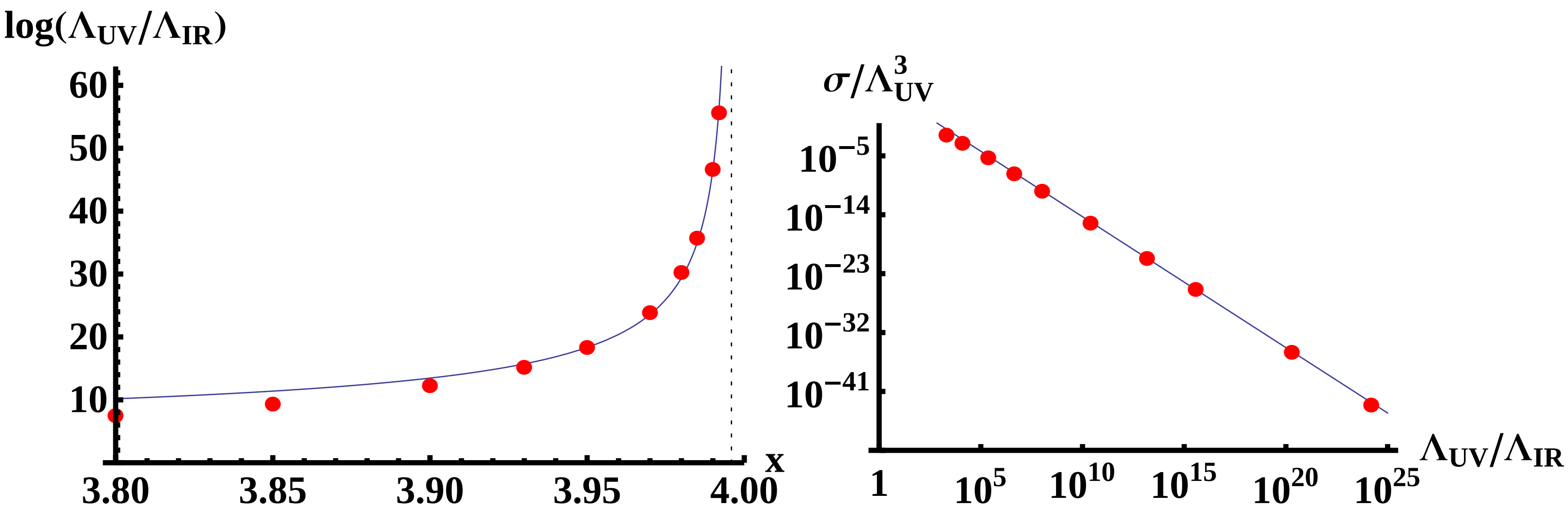

Left: $\log(\Lambda_{\rm UV}/\Lambda_{\rm IR})$ as a function of x (dots), compared to a BKT scaling fit (solid line). Right: σ/Λ^3 plotted against $\Lambda_{\rm UV}/\Lambda_{\rm IR}$ on log-log scale.

Detailed plan of the presentation

- Title page 0 minutes
- Bibliography 1 minutes
- Introduction 2 minutes
- The holographic models:glue 4 minutes
- YM entropy 5 minutes
- YM trace 6 minutes
- The speed of sound 7 minutes
- The holographic models:flavor 9 minutes
- The chiral vacuum structure 12 minutes
- Chiral restauration at deconfinement 14 minutes
- Jump of the condensate at the phase transition 16 minutes
- Meson Spectra 18 minutes
- Mass dependence of f_π 19 minutes
- Linear Regge trajectories 20 minutes

- The Veneziano Limit 22 minutes
- The Banks-Zaks region 24 minutes
- Fusion 26 minutes
- The effective potential 30 minutes
- Condensate dimension at the IR fixed point 32 minutes
- Below the BF bound 35 minutes
- Matching to QCD : UV 36 minutes
- Matching to QCD : IR 41 minutes
- Varying the model 43 minutes
- Comparison to previous guesses 44 minutes
- Holographic β-functions 47 minutes
- Parameters 48 minutes
- UV mass vs T_0 and r_1 54 minutes
- The free energy 56 minutes
- Outlook 58 minutes